Fig. 5.10 Dilatometric data: (a) direct transformation below the bainite–start temperature; (b) two–stage heat–treatment in which the initial transformation to allotriomorphic ferrite is followed by further transformation below B_S;(c) as in (b), but with an elevated temperature anneal imposed between the allotriomorphic and bainitic transformation to homogenise carbon in the residual austenite (see overleaf).

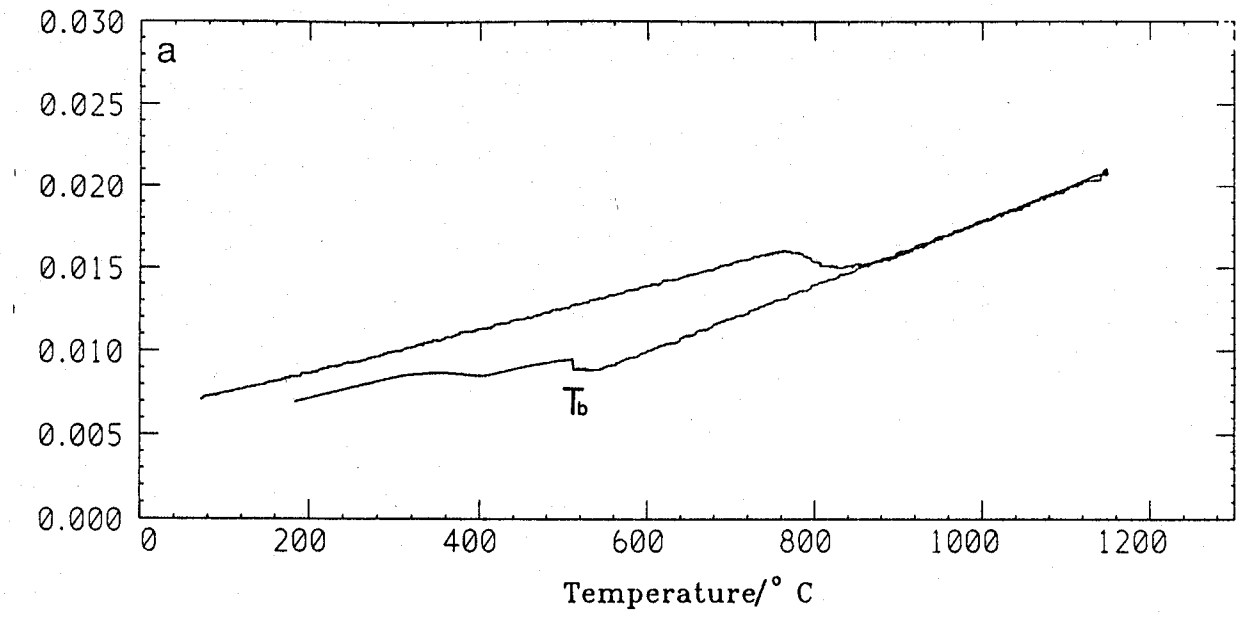
a
0.030
0.025
0.020
0.015
0.010
0.005
0.000
0
200
400
600
800
1000
1200
Tb
Temperature/° C

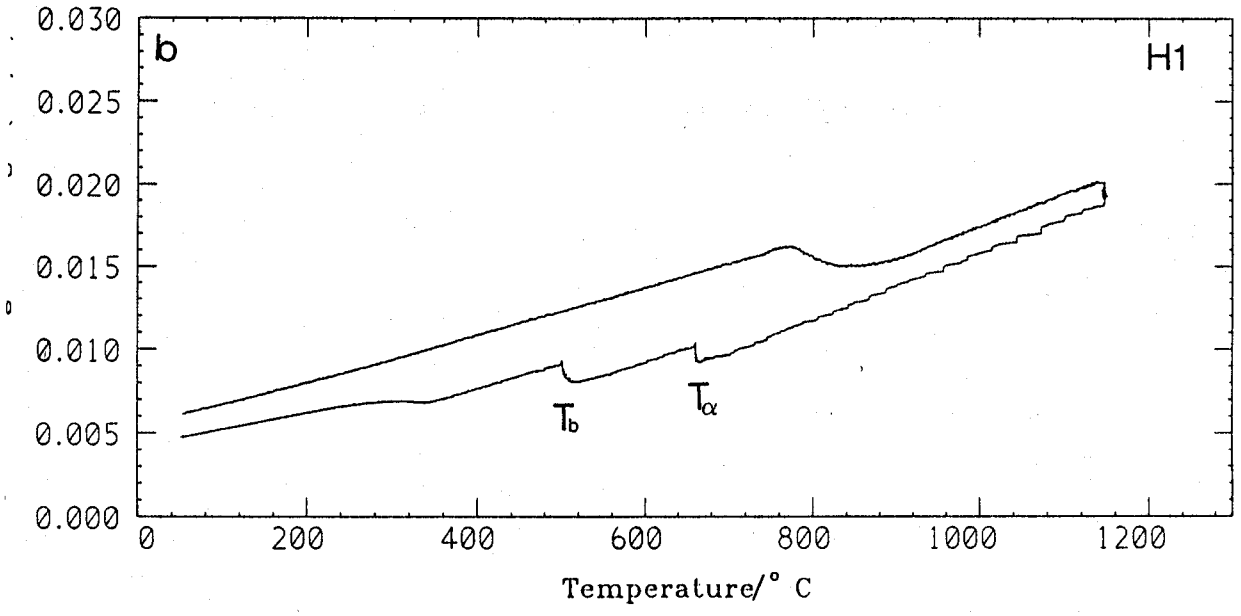
b
H1
0.030
0.025
0.020
0.015
0.010
0.005
0.000
0
200
400
600
800
1000
1200
Tb
Tα
Temperature/° C

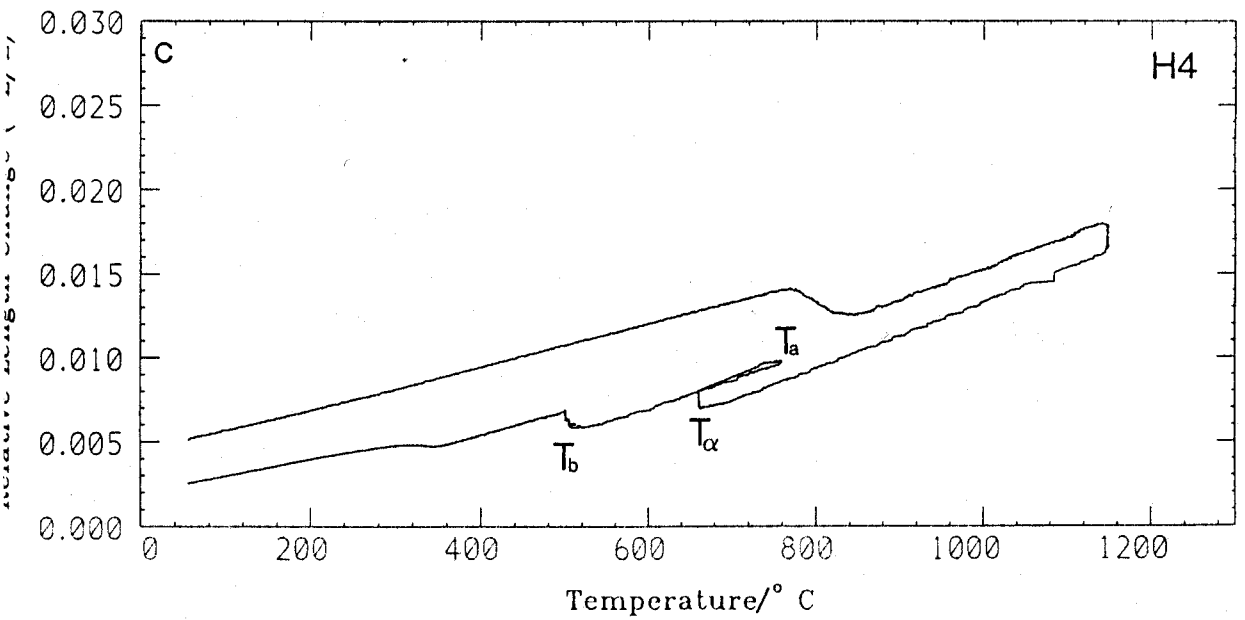
c
H4
0.030
0.025
0.020
0.015
0.010
0.005
0.000
0
200
400
600
800
1000
1200
Ta
Tb
Tα
Temperature/° C

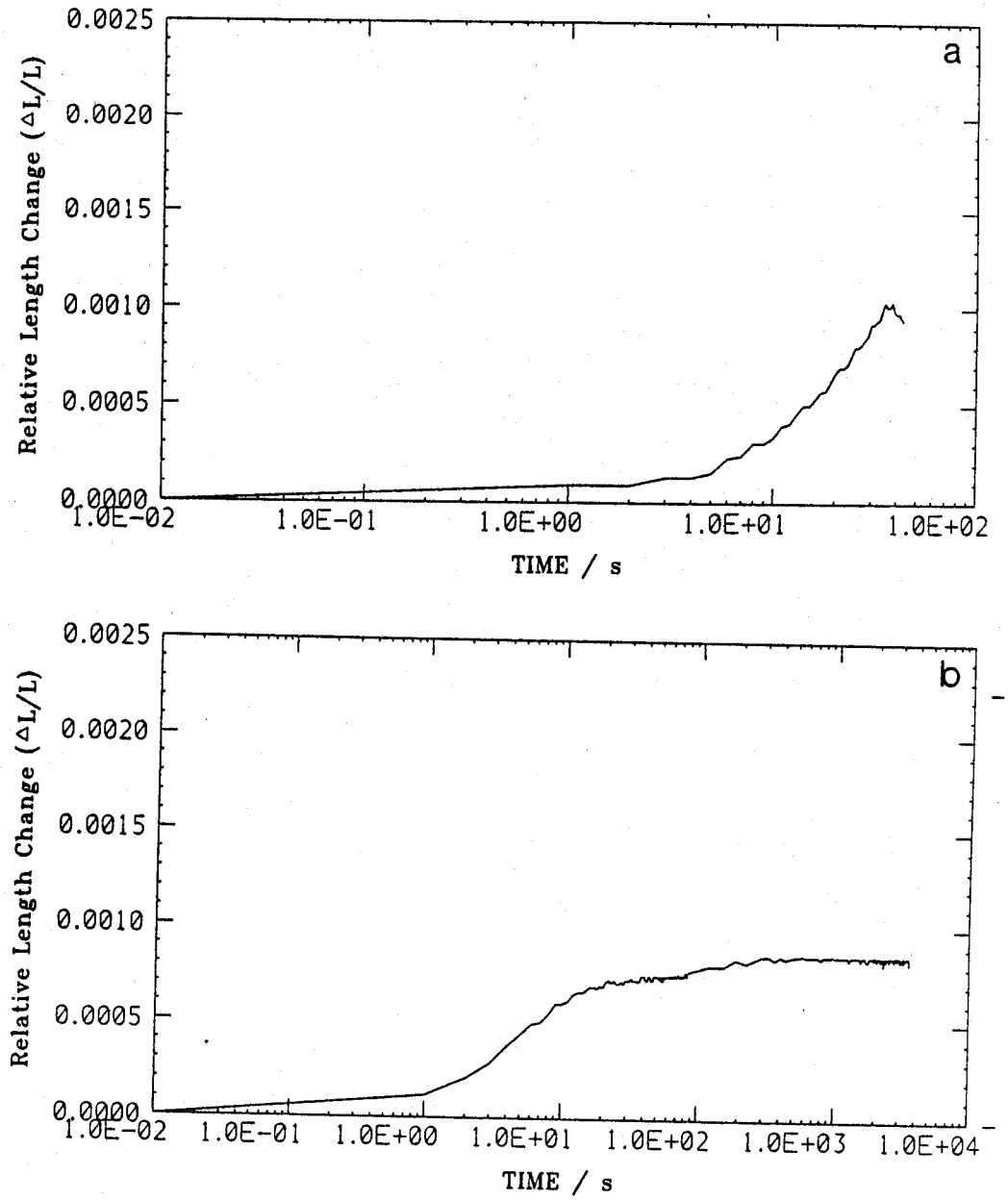

Fig. 5.11 **(a)** Dilatometric data showing that substantial transformation begins after about 10 s at 660 °C, consistent with the calculated TTT diagram of Figure 5.1. **(b)** Illustration of the fact that isothermal transformation within the bainite temperature range leads to a fairly rapid cessation of reaction, permitting the carbon concentration of residual austenite at that stage to be compared against the T_o' phase boundary.

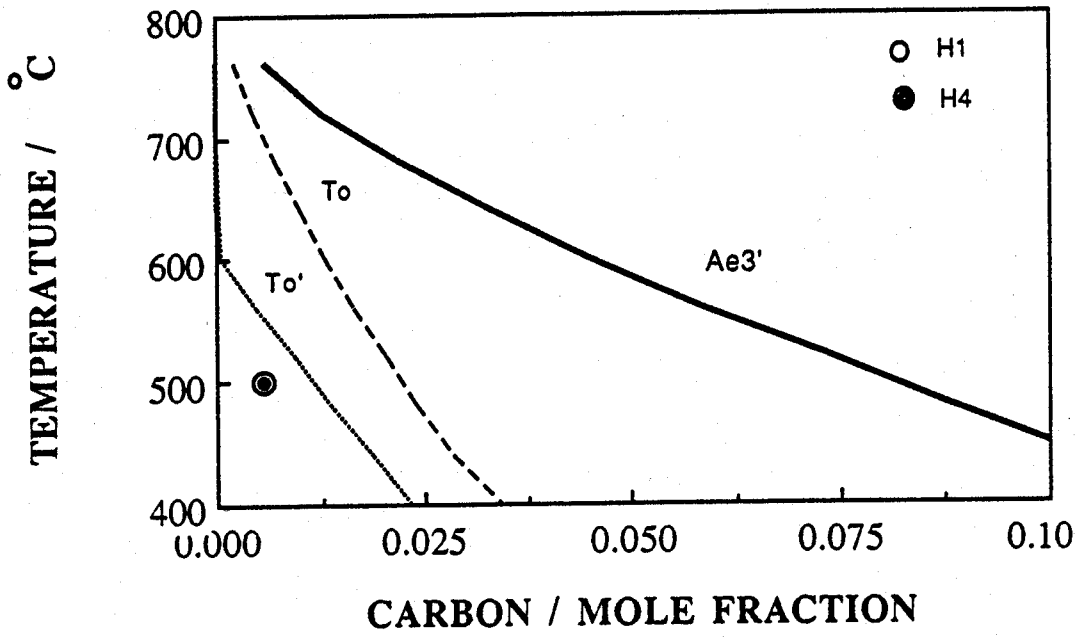

Fig. 5.12 The carbon concentrations of the austenite that is left untransformed after the cessation of the acicular ferrite or bainitic transformation (in a mixed microstructure which also contains some allotriomorphic ferrite), plotted together with calculated phase boundaries. The transformations clearly cease well before the austenite reaches its paraequilibrium or equilibrium composition.

Chapter 6

Continuous Cooling Transformation Characteristics of Fe-Cr-C Reheated Weld Metals

6.1 Introduction

The work so far explains the transition from acicular ferrite to bainite, in the case of Fe-Cr-C weld metals (see chapter 4) and indeed is consistent with other published results of Horri *et al.*, (1988), Grong *et al.*, (1986) and Harrison and Farrar (1987a,b). Thus, acicular ferrite can be encouraged by introducing a controlled layer of allotriomorphic ferrite all along the austenite grain boundaries. This chapter is a first step towards the application of these concepts to practical weld situations.

Some published data suggest that the acicular ferrite plate size, in a mixed microstructure of α_a and $\alpha_,$ is a function of the austenite grain size (Dallam and Olson, 1989, Fleck *et al.*, 1986). Coarser austenite grains lead to finer plates and vice versa. It also appears that a sample with finer acicular ferrite showed better toughness characteristics. An explanation for these observations is as follows: the ratio of the allotriomorphic ferrite thickness to austenite grain size changes (q_α/R_γ) is a function of the volume fraction of ferrite. Allotriomorphic ferrite growth involves the partitioning of solutes. In the case of welds, transformation proceeds mainly by a paraequilibrium mechanism, so that the solute partitioning is carbon. Dallam and Olson assumed that the partitioned carbon is uniformly distributed in the residual austenite, which will then have a reduced free energy for transformation to ferrite. This stabilisation of the austenite by carbon enrichment may somehow lead to different transformation kinetics and hence different plate size..

This assumption of a homogeneous residual austenite is not justified from the work presented in chapters 4 & 5, which shows that there is a large concentration near the austenite-allotriomorphic ferrite interface within the time scale of the experiments typical of welding. This chapter describes the results of a series of experiments carried out to change the ratio of allotriomorphic ferrite to austenite grain size, to check the hypothesis of Dallam and Olson. The allotriomorphic ferrite thickness was changed while keeping the austenite grain size constant. The aim was to observe the effect on the acicular ferrite that forms subsequently.

The second feature of the experiments involved the study of the transformation to acicular ferrite during continuous cooling experiments to simulate the behaviour during welding. In practice the welding conditions have to be selected so that a small amount of allotriomorphic ferrite grows before the B_s temperature is reached.

Table 6.1 Details of step heat treatments:

Experiment	Alloy	T_1, °C/ time at T_1, s	T_2, °C/ time at T_2, s
A78ST1	78	700 / 15	530 / 30
A78ST2	78	700 / 30	530 / 30
A78ST3	78	700 / 45	530 / 30
A77ST1	77	700 / 90	500 / 30
A77ST2	77	700 / 120	500 / 30
A77ST3	77	700 / 240	500 / 30

6.2 Experimentation

As mentioned above, the aim was to examine the effect of carbon partitioning during allotriomorphic ferrite formation on the subsequent transformation to acicular ferrite. Alloys 77 and 78 (Table 2.2), which differ in chromium concentrations, were used, the preparation techniques being described in chapter 2.

Table 6.1 describes the step heat treatments, where the residual austenite carbon concentrations were expected to change with different transformation times at T_1. The heat treatments were carried out using the *Theta-Industries* high speed dilatometer. In all cases the austenitisation temperature was 1150 °C and time was 10 minutes. The austenite grain size for this treatment was measured to be around 78 μm $\pm$ 10. The transformation temperature T_2 (below B_s where acicular ferrite can nucleate on inclusions) and time at T_2 were kept the same for a particular alloy composition. The time at T_2 was chosen to be small to avoid extensive growth. The cooling between T_1 and T_2 was achieved using a helium gas jet. Partial transformation at T_2 followed by quenching to ambient temperature facilitated the identification of ferrite plates. The nucleation density of acicular ferrite was estimated by counting the plates in a square grid of 20 $\times$ 20 μm . Table 6.2 summarises the continuous cooling transformation studies. The hardness was measured using a *Leitz* microhardness tester with a force of 0.981 N.

6.2.1 Interpretation of Dilatometric Data:

The relative length change $\frac{\Delta L}{L}$ *vs* temperature (T) curve was differentiated numerically with respect to temperature. The slope was calculated by regressing over 10 points on each side of the temperature of interest. The interval between each point being 1 °C. The differentiated curve is expected to show a constant value e_γ in the absence of transformation and another constant value e_α when transformation is completed. The transformation start and finish temperatures

Table 6.2 Continuous cooling transformation experiments:

Experiment	Alloy	Cooling Rate $°Cs^{-1}$
A78CCT1	78	5
A78CCT2	78	20
A78CCT3	78	50
A77CCT1	77	1
A77CCT2	77	5

can be measured from the deviations from constancy. Previous researchers on CCT behaviour of steel have used $\frac{\Delta L}{L}$ versus T curve directly to measure these points (Lee and Hon 1987, Ferrante and Farrar, 1982 and Farrar and Harrison, 1987). Eldis (1977) pointed out the uncertainty of measuring the transformation finish temperatures of bainite. The bainite and acicular ferrite can transform from carbon enriched austenite below the M_s, of the average alloy composition. Hence, a temperature at which the maximum rate of transformation takes place, T^i is measured as a parameter characterising the acicular ferrite or bainite reaction.

6.3 Results

Samples with differing ratios of allotriomorphic ferrite thickness to austenite grain size (q_α/R_γ) revealed no systematic change in the number density of acicular ferrite plates (Fig. 6.1). The measured densities of acicular ferrite plates are presented in Table 6.3. The table also contains the volume fraction of allotriomorphic ferrite. The diffusion distance when allotriomorphic ferrite growth stopped (the distance for the carbon composition to drop from $x_c^{\gamma\alpha}$ to $\bar{x}_c$ in front of the α/γ interface) was calculated using equation 4.3. Calculations were carried out for A78ST3 and A77ST3. The effective diffusion distance was found to be 14 and 17 μm so that a substantial region in front of the interface should be transformation free. Figure 6.2 shows the transformation free zone near to the α/γ interface. The zone dimensions are comparatively smaller than the diffusion distance values calculated, because the transformation to bainite is stifled near to the transformation interface, the dimensions of which are much smaller than the diffusion distance.

Figure 6.3 shows the measured $\frac{\Delta L}{L}$ *vs* T curves and the corresponding numerically differentiated curves of the continuous cooling transformation experiments. The transformation start and finish temperatures were measured from these graphs (Table 6.4). The corresponding micrographs are presented in Fig. 6.4. The relative length change plots of A77CCT1 and

Table 6.3 Measured thickness of allotriomorphic ferrite and acicular ferrite plate density.

Experiment	allotriomorphic ferrite		acicular ferrite
	half thickness	volume	plate density
	μm	%	μm $^{-2}$
A78ST1	3-5	12	0.05 ± 0.005
A78ST2	6-9	22	0.0475± 0.0125
A78ST3	10-12	35	0.07 ± 0.0125
A77ST1	1-3	10	0.05 ± 0.0075
A77ST2	5-8	19	0.065 ± 0.0075
A77ST3	12-15	37	0.07 ± 0.0125

A77CCT2 are presented in Fig. 6.5 and corresponding microstructures in Fig. 6.6. The micrographs clearly show that for the higher cooling rates the austenite grain boundaries are only partially decorated with allotriomorphic ferrite, causing a bainitic microstructure. A detailed study of the microstructures of A78CCT2 and A78CCT1 indicated an apparent change in plate size. The plate size of A78CCT1 (5.3 ± 0.8) was higher than the plate size of A78CCT2 (4.1 ± 0.6), measured using the random mean linear intercept technique on optical micrographs, and corresponding hardness values were found to be 273 HV and 286 HV respectively.

Table 6.4 Characterisation of continuous cooling experiments. The parameters are discussed in the text.

Exp	$\Delta t_{800-500}$	Allotriomorphic ferrite	$T^i_{acic/bain}$
No	seconds	$T_s - T_e$ °C†	
A78CCT1	76	740-640	600
A78CCT2	25	710-615	565
A78CCT3	21.5	710-640	585
A77CCT1	300	760-620	545
A77CCT2	60	750-650	520

†$T_{s,e}$ stand for start and end transformation temperatures.

6.4 Discussion

The results show that the enrichment of austenite takes place only locally, near the α/γ interface as supported by the transformation free zones observed near to the interface (Fig. 6.2). Thus, the reported variation of plate size by Dallam and Olson (1989) and the results of Fleck *et al.*, (1986) still remains to be explained.

On the other hand, the microstructure of the continuously cooled specimens showed an apparent change in the acicular ferrite plate size. A78CCT1 (slow cooling rate) showed coarse plates when compared with A78CCT2 (high cooling rate). The scale of the size variation is comparable to variations published by Dallam and Olson (1989) and Fleck *et al.*, (1986). Coarser acicular ferrite was associated with higher T^i_{acic}=600 °C compared to finer acicular ferrite size T^i_{acic}=560 °C. The allotriomorphic ferrite was found to be around 25% in the case of A78CCT1 compared with 14% in the case of A78CCT2. The volume fractions are smaller, so the plate size variation cannot be attributed to the enrichment of austenite. The results indicate, however, that there is a strong relation between the transformation temperature and the acicular ferrite plate size. This result is similar to the reported variation of plate size with transformation temperature for bainitic laths (Ohmori *et al.*, 1971). Thus the development of acicular ferrite plates show another similarity with bainite.

Irrespective of the mechanism of the reduction of plate size, the results showed that the finer acicular ferrite is associated with a lower transformation temperature. Thus, welds should be designed in such a way that the maximum extent of transformation occurs at lower transformation temperatures. This can be achieved in welds only by increasing the cooling rate or altering the alloy chemistry. Too large a cooling rate causes a transition from acicular ferrite to bainite (A78CCT3, Fig. 6.5 & A77CCT2, Fig. 6.6). The results are consistent with diagrams published by Harrison and Farrar (1987b), who found that an increased cooling rate leads to an abrupt increase in volume fraction of bainitic ferrite (referred to as lath ferrite), with a drop in allotriomorphic ferrite (Fig. 6.7).

6.5 Conclusions

Changes in the acicular ferrite plate size during continuous cooling are probably due to corresponding changes in transformation temperatures rather than due to any enrichment of the austenite by prior transformation to allotriomorphic ferrite.

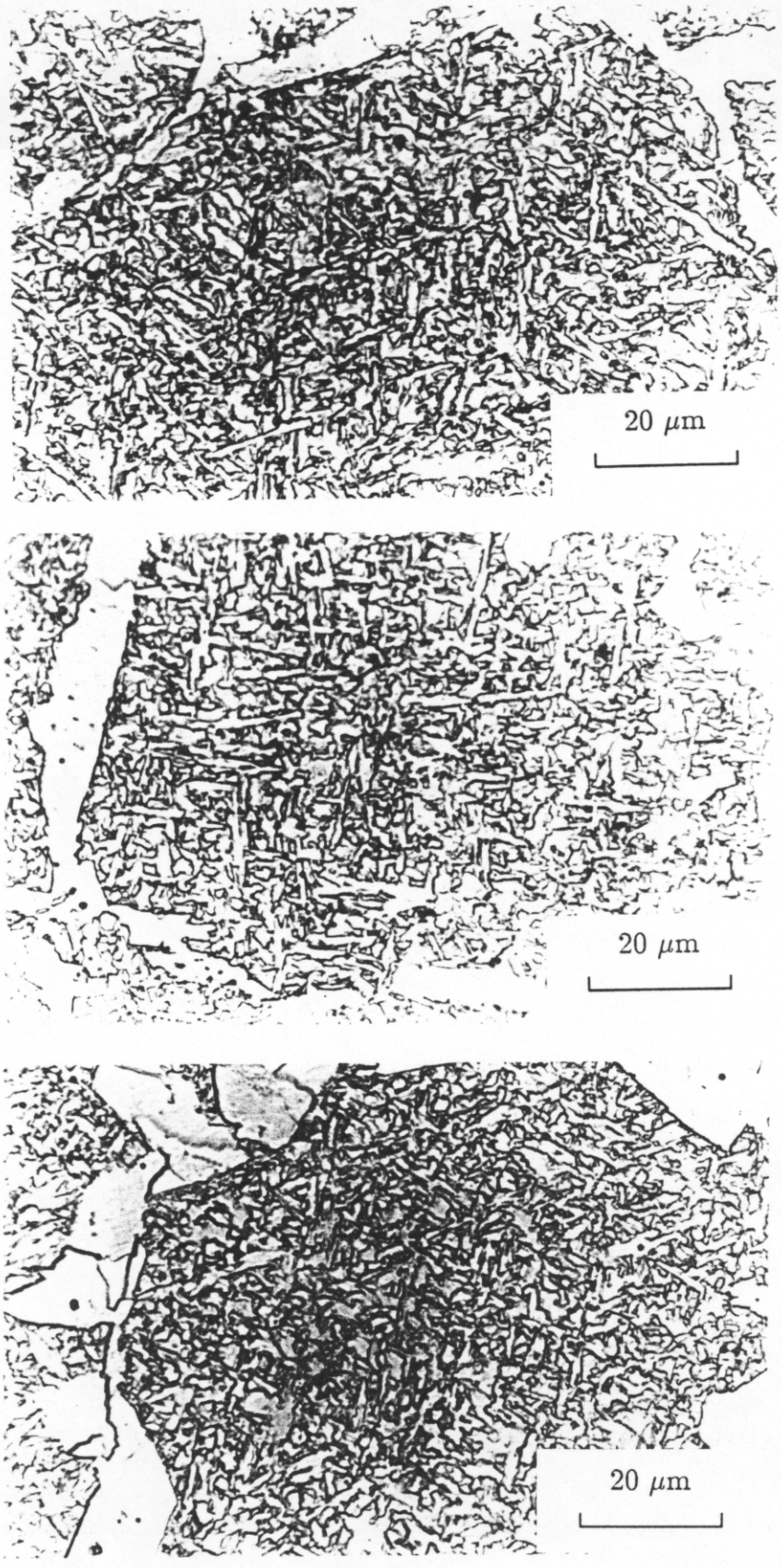

Fig. 6.1 The microstructure obtained after step heat treatments (Table 6.1). The microstructures show no apparent change in number of acicular ferrite plates per unit area. (a) A78ST1, (b) A78ST2, (c) A78ST3.

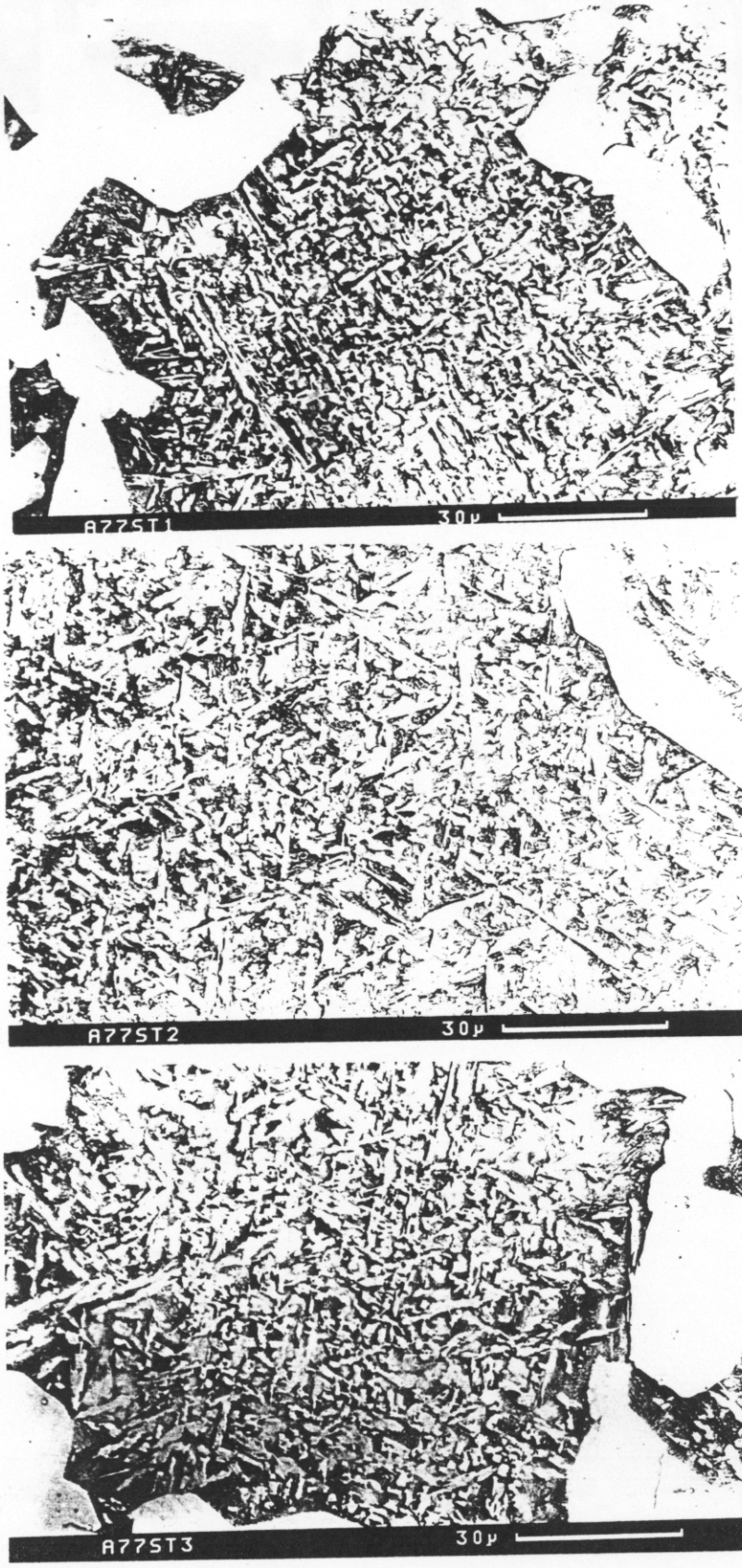

Fig. 6.1 continued

(d) A77ST1, (e) A77ST2, (f) A77ST3.

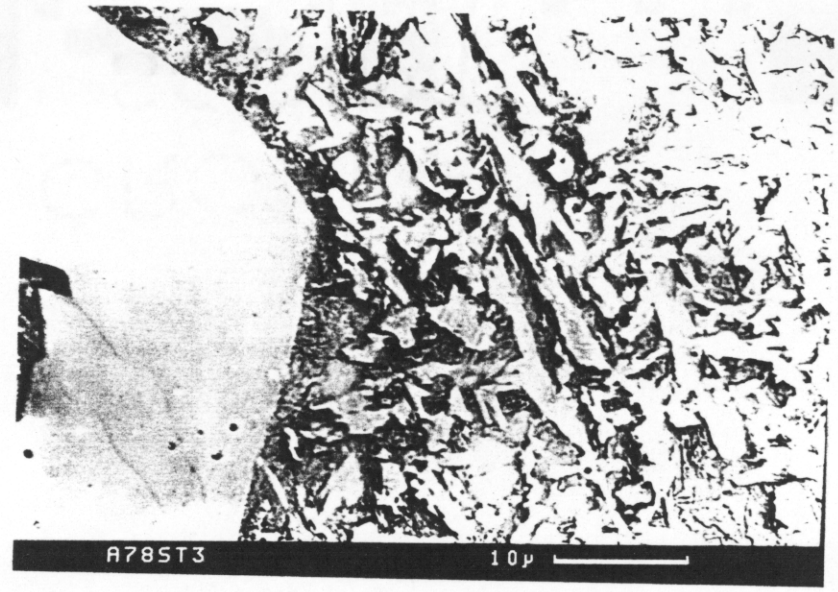

a

b

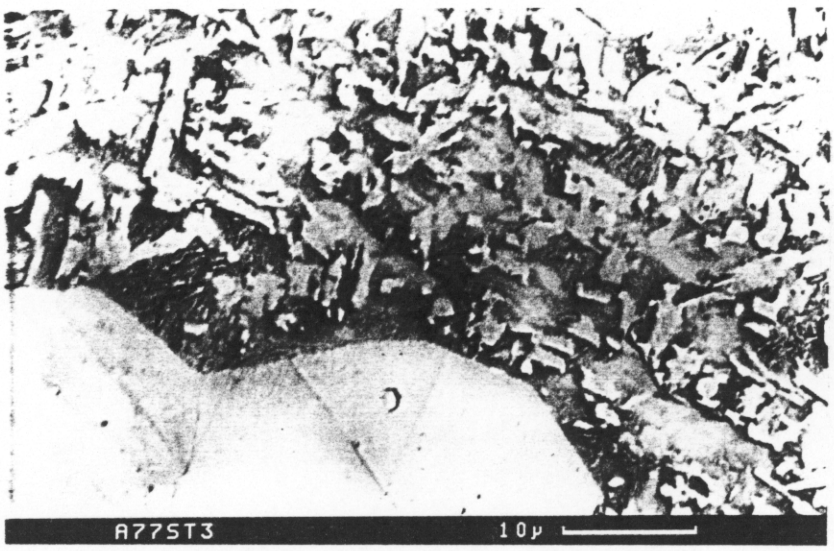

Fig. 6.2 The microstructure of (a) A78ST3 and (b) A77ST3 indicating a transformation free zone near to α/γ interface. Dark regions are the martensite transformed from the enriched austenite near to the interface.

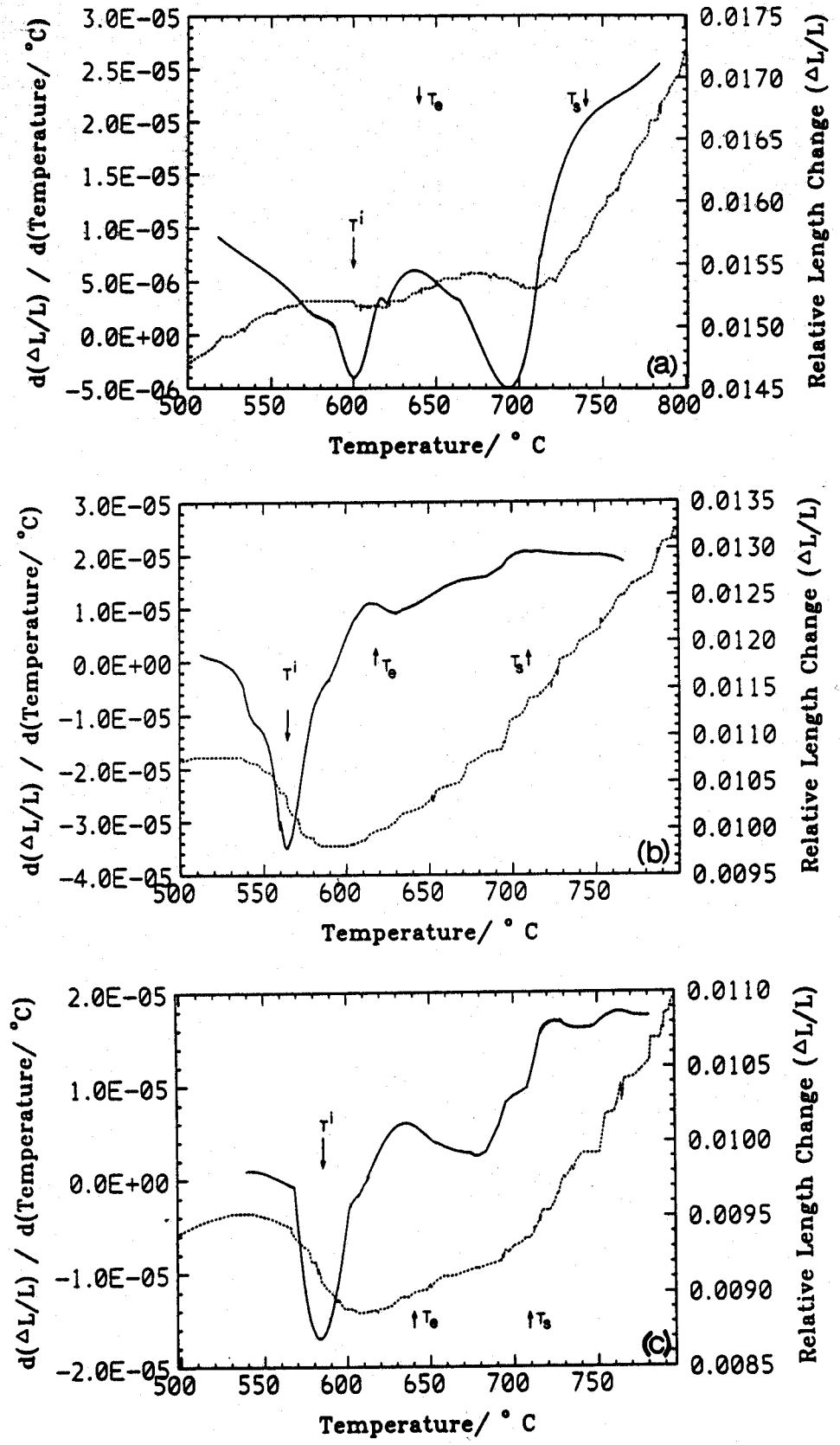

Fig. 6.3 The plots of relative length change, $\frac{\Delta L}{L}$ with temperature, T. The solid lines are numerically differentiated curves and the dotted lines are the original curves. The allotriomorphic ferrite transformation start and end temperatures are marked. The inflection temperature point for acicular ferrite reaction is also marked. The plots clearly show the transformation sequences of allotriomorphic ferrite and acicular ferrite. (a) A78CCT1, (b) A78CCT2, (c) A78CCT3.

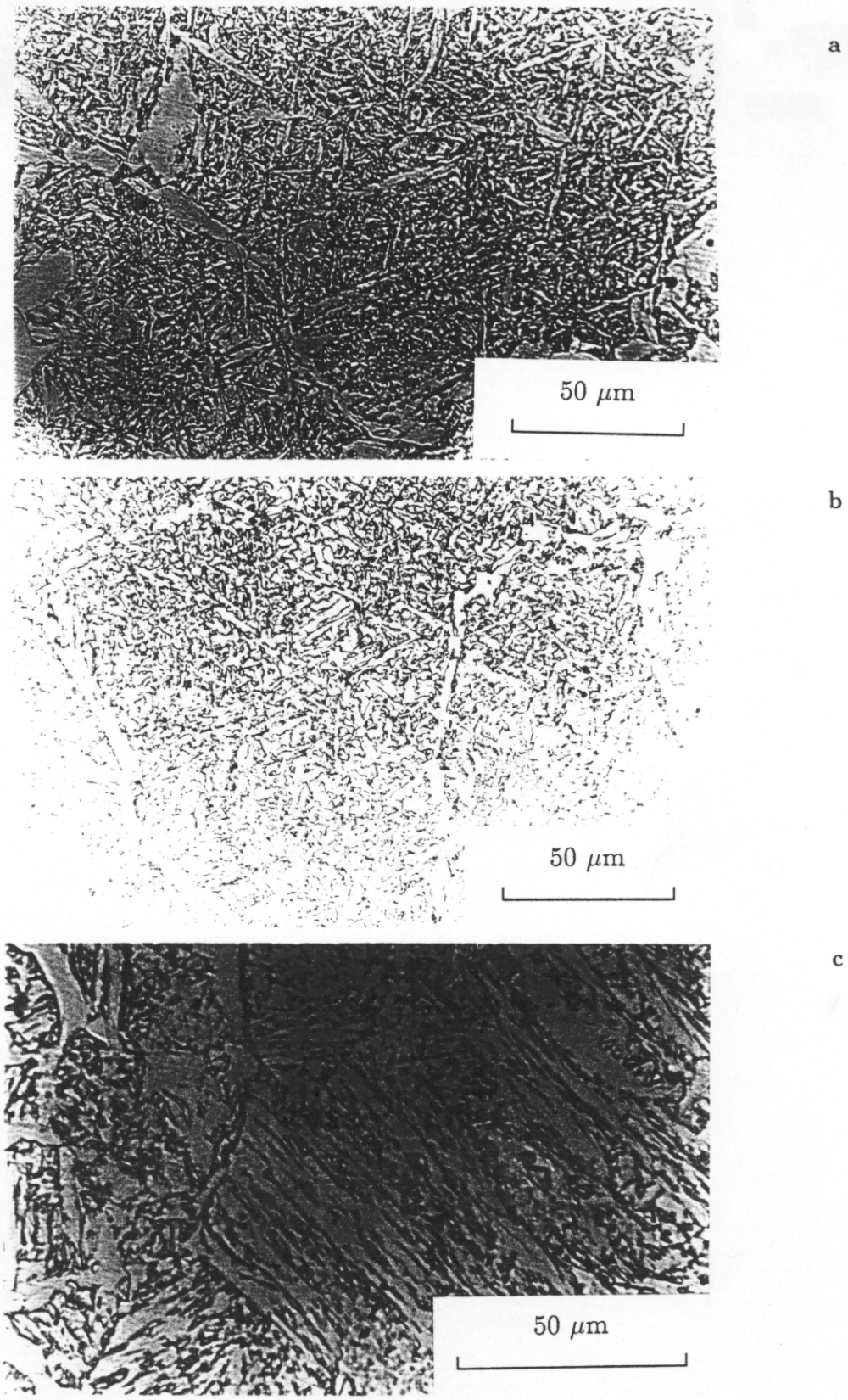

Fig. 6.4 The microstructure corresponding to the continuous cooling transformation experiments in alloy 78 (see Table 6.2). Note the development of bainite in the case of A78CCT3 and also the apparent change in plate size with A78CCT2 and A78CCT1. (a) A78CCT1, (b) A78CCT2, (c) A78CCT3.

a

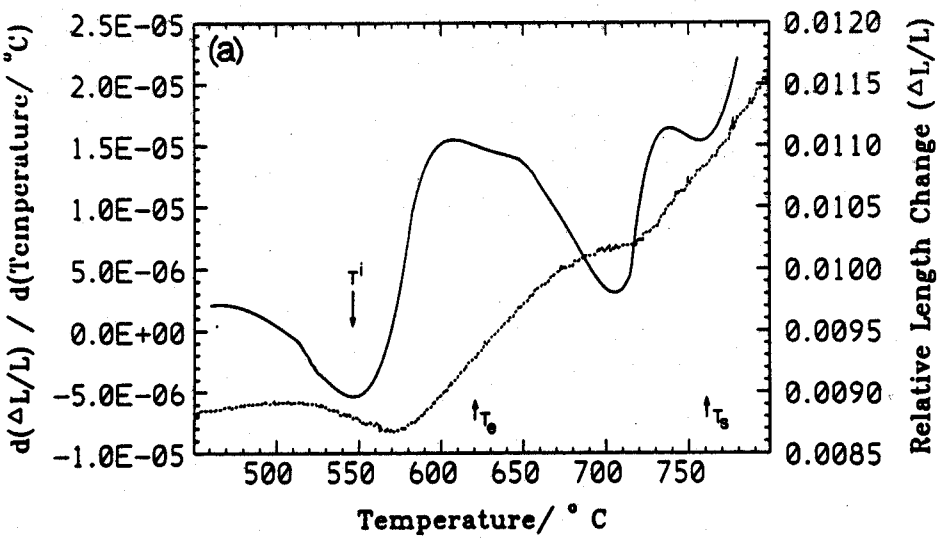

b

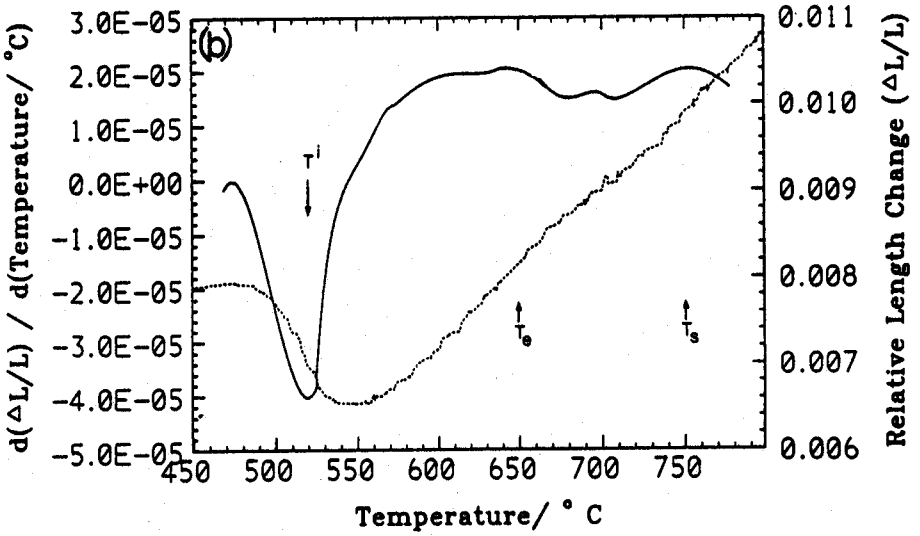

Fig. 6.5 The plots of relative length change, $\frac{\Delta L}{L}$ with temperature, T. The solid lines are numerically differentiated curves[5] and the dotted lines are original curves.[6] (a) A77CCT1, (b) A77CCT2.

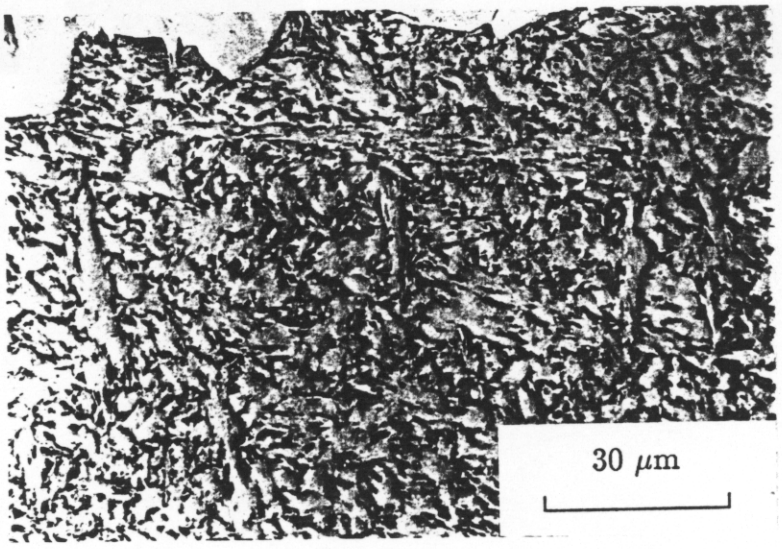

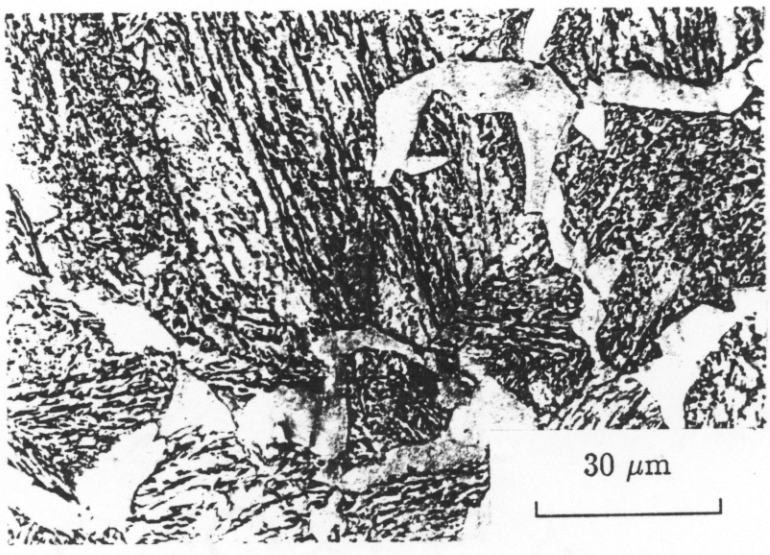

Fig. 6.6 The microstructure corresponding to the continuous cooling transformation experiments in alloy 77 (see Table 6.2). (a) A77CCT1, (b) A77CCT2.

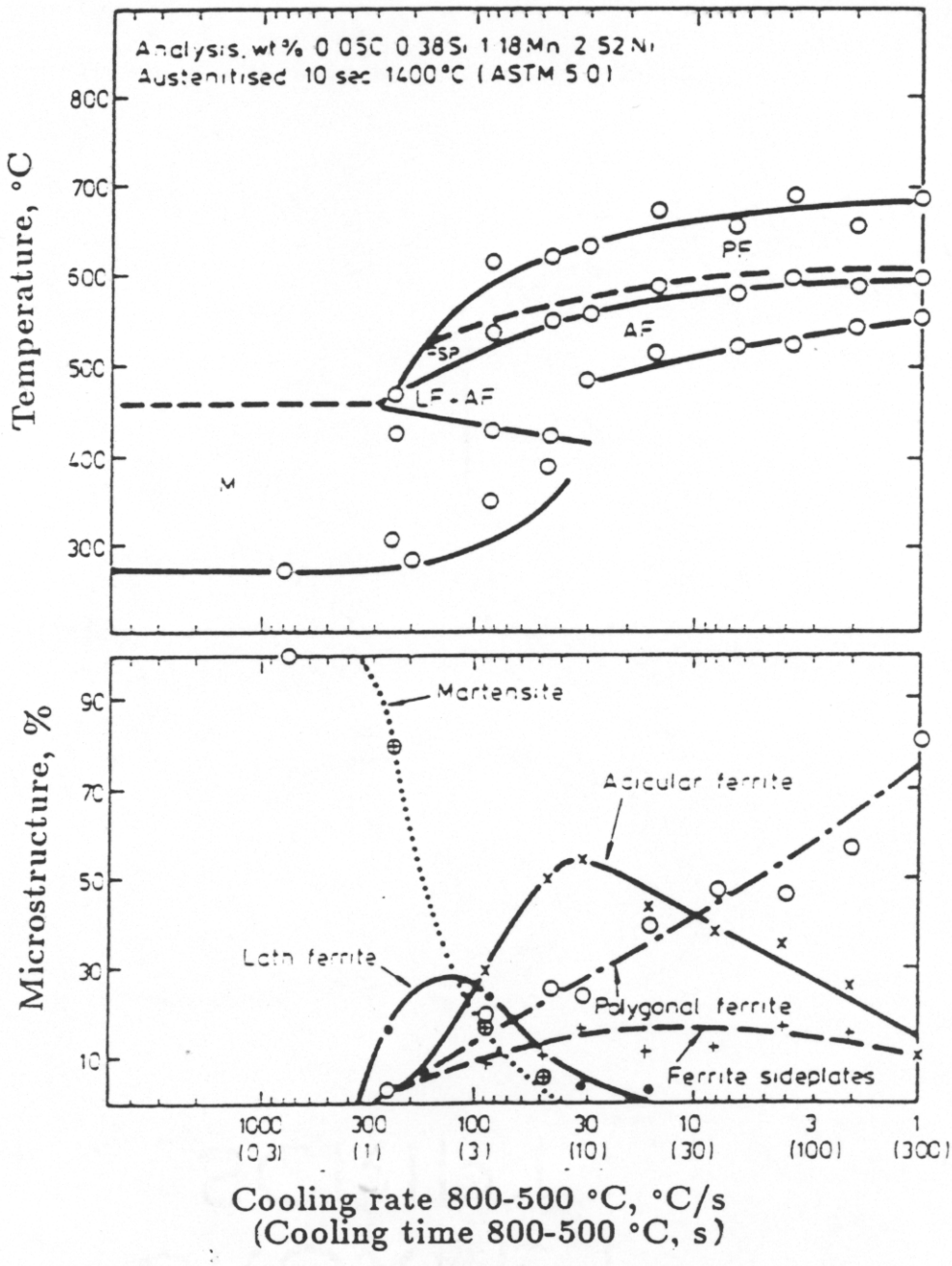

Fig. 6.7 Published CCT and microstructural development diagram of Harrison and Farrar (1987b), indicating the sensitivity of the acicular ferrite reaction to $\Delta t_{800-500}$.

Chapter 7

A Direct Study of Grain Boundary Allotriomorphic Ferrite Crystallography

7.1 Introduction

The work presented in the previous chapters has emphasised a beneficial role of thin layers of allotriomorphic ferrite layers on removing the austenite grain surfaces as potential nucleation sites for bainite, and hence forcing a microstructural transition from bainite to acicular ferrite when suitable intragranular nucleation sites are available in sufficient numbers (Fig. 4.13c). This beneficial effect of allotriomorphic ferrite has to be balanced against its undesirable ability to stimulate the formation of Widmanstätten ferrite or bainite.

When Widmanstätten ferrite grows from allotriomorphic ferrite, it is contiguous with the latter. Thus, allotriomorphic ferrite can only develop into Widmanstätten ferrite if it has the "right" orientation relationship with the austenite, since Widmanstätten ferrite is a product of displacive transformation. This orientation lies within the so-called "Bain region", within which no plane or direction is rotated by more than about 11° from the Bain orientation (Crosky *et al.*, 1980). The classical Kurdjumov-Sachs (KS) and Nishiyama-Wasserman (NW) orientation relationships lie within this region. The crystallography of allotriomorphic ferrite is therefore of crucial importance in determining whether its presence will have the desired effect of facilitating intragranular nucleation of acicular ferrite, or the undesirable effect of providing a substrate for the nucleation of Widmanstätten ferrite. It is almost certain that grain boundary allotriomorphic ferrite, when it nucleates, has a good fitting orientation relationship (within the Bain region) with one of the austenite grains with which it is in contact. The ferrite grows, however, by reconstructive transformation. The rate of growth would be faster at incoherent interfaces, *i.e.*, in those austenite grains with which the ferrite is "randomly" orientated. The growth process could thus lead to a situation in which the majority of allotriomorphic ferrite/austenite interface is incoherent and hence incapable of developing into Widmanstätten ferrite.

The purpose of the present work was to determine the fraction of ferrite allotriomorphs which, as a consequence of the wrong crystallography generated by selective growth, are unlikely to lead to Widmanstätten ferrite formation. Similar crystallographic experiments have been reported previously (King and Bell, 1975), but the austenite orientation was deduced indirectly by assuming specific habit plane indices for Widmanstätten ferrite plates, indices which are now known to be different (Watson and McDougall, 1973). Experiments have been designed here which allow the retention of large quantities of austenite permitting the direct measurement of its orientation.

7.2 Experimental Methods

7.2.1 Alloys and Heat Treatment

The chemical compositions (wt.%) of the two Fe–C–Si–Mn alloys studied are given in Table 7.1. The steels were prepared as 20 kg vacuum induction melts from high purity base materials. The ingots were forged and hot rolled to 10 mm diameter rods, followed by swaging to 3 mm diameter rods. They were then homogenised at 1200 °C for 3 days while sealed in quartz capsules containing pure argon.

In low alloy steel, usually on cooling to room temperature, there will be very small amounts of retained austenite. The aim of the present work has been to study the crystallography of allotriomorphic ferrite directly with austenite. Hence, the steel studied is of wrought alloy and different composition from the alloy used in previous chapter. The relatively high silicon concentration of the alloys ensures that carbides do not precipitate during the formation of upper bainite (Bhadeshia and Edmonds, 1979). Consequently, the carbon that is partitioned into the residual austenite stabilises it to further transformation, with substantial quantities of austenite being retained to ambient temperature. This austenite is of value in directly assessing the crystallography of any transformation products. Two–stage step heat treatments were designed to take advantage of this characteristic, to obtain mixed microstructures of allotriomorphic ferrite, bainitic ferrite and retained austenite. After austenitisation, the samples were partially isothermally transformed to a small volume fraction of allotriomorphic ferrite at a temperature T_1, followed by a second isothermal heat treatment at a lower temperature T_2 in order to induce the formation of upper bainitic ferrite. The amount of allotriomorphic ferrite was kept small in order to study the early stages of the reaction, before impingement between different allotriomorphs can confuse interpretation. Consequently, it is the subsequent growth of bainitic ferrite which leads to a larger extent of carbon enrichment in the residual austenite, necessary to prevent much of the untransformed austenite at T_2 from decomposing martensitically during the final quench to ambient temperature. The treatment at T_1 was in some cases omitted in order to study the crystallography of bainite in its own right.

7.2.2 Metallography

Thin foil samples for transmission electron microscopy were prepared using the procedure outlined in chapter 2. The samples were examined in *Philips* EM300 and EM400T transmission electron microscopes operated at 100 and 120 kV respectively.

Figure 7.1a shows the optical micrograph of allotriomorphic ferrite along the austenite grain boundaries and Fig. 7.1b shows typical bainitic sheaves observed within the austenite grain grains. Microanalysis experiments were carried out on the EM400T, using an energy

Table 7.1 Chemical composition (wt.%) and details of the heat treatments. The austenitisation conditions were 1000 °Cand for 5 minutes.

Alloy	C	Si	Mn	T_1 °C/Time	T_2 °C/Time
A1	0.40	2.03	3.00	703/10 h	340/12 h
A2	0.22	2.03	3.00	640/ 1 h	340/140 min

dispersive X-ray analysis facility. The specimens, which were about 100 nm thick, were held in a beryllium holder tilted 35° from the normal. The X-ray count rate was optimised at about 1000 counts s^{-1}, over a count period of 100 s. The data were analysed using the *LINK RTS 2 FLS* program for thin foil microanalysis; this corrects the data for atomic number and absorption effects and accounts for overlapping peaks by fitting standard profiles. Even though the probe diameter was about 2-5 nm, beam spreading due to the scattering of electrons within the thin foil gave an estimated broadened beam diameter of about 20 nm, a size which was small enough for the purposes of the investigation.

7.3 Crystallographic Technique

Austenite/ferrite orientations outside the Bain region generally arise during reconstructive transformation in which growth is not restricted by austenite grain boundaries, so that a particle can grow into regions which had little or no influence in determining its orientation during the nucleation stage. Although the ferrite may nucleate from austenite with an orientation within the Bain region, it can then grow with a random orientation into adjacent austenite grains. The probability of finding ferrite which is well related to the adjacent austenite depends therefore on the growth stage; the aim here is to detect whether or not the orientation of ferrite which has grown well beyond the nucleation stage has an orientation within the Bain region, since only then is it capable of nucleating secondary Widmanstätten ferrite plates. To distinguish the Bain region from random orientations does not require extreme precision of the kind associated with Kikuchi line measurements. The experimental data presented here are based on an analysis of the reciprocal lattice vectors observed in conventional selected area electron diffraction patterns. The zone axis of each pattern can then deviate typically by 5° from the optic axis of the microscope, and this can be used as an estimate of the error. In fact, the error should be somewhat smaller since the orientations were deduced not from the zone axes, but by examining the relationship between pairs of reciprocal lattice vectors (in the same diffraction pattern) from each of the two crystals concerned. The four reciprocal lattice vectors

were then used to determine the coordinate transformation matrix defining the orientation relationship, in the manner described elsewhere (Yang and Bhadeshia, 1989a and Bhadeshia, 1987b).

The validity of the method was checked by measuring the orientation relationship between bainitic ferrite and its parent austenite; the displacive transformation mechanism ensures that the orientation should always lie well within the Bain region, with a pair of corresponding close–packed planes and a pair of corresponding close–packed directions within those planes being approximately parallel. Data from 16 sets of measurements are summarised in Fig. 7.2, where the angle between the close–packed planes $\{111\}_\gamma$ and $\{011\}_\alpha$ is designated θ, and that between the directions $< 10\bar{1} >_\gamma$ and $< 11\bar{1} >_\alpha$ is designated ϕ. The data are, as expected, all within the Bain region. The mean value of the angle θ was found to be 2.5° with a standard deviation of 1.9° whereas the corresponding mean and standard deviation for ϕ were 3.4 and 2.0° respectively. Given that θ is expected to be very close to zero (within about 0.5°), the analysis confirms that the error associated with the technique is small enough to distinguish between random and Bain–region orientations.

7.4 Results and Discussion

7.4.1 Allotriomorphic Ferrite/Austenite Orientation Relations

Figure 7.3 revealed that the two–stage heat treatment resulted in the desired microstructure, consisting of small allotriomorphs of ferrite at the austenite grain boundaries, and sheaves of bainitic ferrite and retained austenite. Facets which appeared to be growth ledges were observed on the allotriomorphic ferrite indicated by the arrow in Fig. 7.3, on the side of the allotriomorph which had a near KS relation with the austenite. An other remarkable example of the crystallographic data obtained using transmission electron microscopy and electron diffraction is presented in Fig. 7.4 which will be discussed in detail after a presentation of all the crystallographic data. Occasionally, the allotriomorphic ferrite in alloy A1 seemed to contain manganese rich, unidentified carbides as seen in Fig. 7.5 and Table 7.2.

The complete set of crystallographic data are presented in Tables 7.3 & 7.4, for alloys A1 and A2 respectively. In these tables, an "a" appearing after the identification number represents the orientation relationship between the allotriomorph and the adjacent austenite grain γ_1, whereas "b" denotes the orientation of the same allotriomorph with respect to the other austenite grain (γ_2) with which it is in contact. We also adopt the convention here that the α/γ_1 orientation is chosen to be the one that is better with respect to lattice matching than the α/γ_2 orientation. In one particular case, where the ferrite was found at a three–grain junction, a letter 'c' was used to identify its orientation with the third austenite grain. The orientation

Table 7.2. Microanalysis data on allotriomorphic ferrite, bainite and carbide on alloy A1 & A2 after step heat treatment. The compositions of the austenite and ferrite in equilibrium were calculated using the National Physical Laboratory MTDATA system (1989). Note the absence of partitioning for bainitic ferrite, confirming the microanalysis technique.

Allotriomorphic ferrite			
Element	Observed	Equilibrium	Alloy
Mn	1.6	1.00	A1 (703 °C)
Si	2.5	2.68	A1 (703 °C)
Mn	1.8	1.16	A2 (640 °C)
Si	1.9	2.40	A2 (640 °C)
Bainitic ferrite			
Element	Observed	Expected	Alloy
Mn	3.1	3.00	A1
Si	2.0	2.03	A1
Mn	3.2	3.00	A2
Si	2.3	2.03	A2
Carbide			
Element	Observed	Expected	Alloy
Mn	12.6	-	A1
Si	0.4	-	A1

data are summarised for convenience in terms of the angles θ and ϕ defined earlier, although the full coordinate transformation matrix which completely defines the α/γ orientation relation was available for each case. They results are also illustrated graphically in Fig. 7.6.

Out of a total of 19 cases examined in detail each case consisting of an allotriomorphic ferrite and its adjacent γ grains, only 7 were consistent with an α/γ_1 orientation relation within the Bain region, the majority of the orientation relationships being more or less random. The seven cases were found to be consistent with the C. S. Smith (1948) hypothesis in that the ferrite in each case revealed a tendency to crystallographically facet on the side with the Bain region related austenite, whereas curved boundaries were apparent on the other side with which it was randomly orientated. In only one case was the ferrite orientation such as to be within the Bain region with respect to both of the adjacent austenite grains within the limits of experimental error (Case 15, Table 7.3).

Only a small fraction of allotriomorphs are therefore found to be in the right crystallographic orientation to provide a substrate for secondary Widmanstätten ferrite growth (the fact that Widmanstätten ferrite did not form is because the alloys were heat-treated above the Widmanstätten ferrite start temperature). It is very likely that this result cannot be attributed to the orientation relationships that develop during nucleation. In order to avoid a large activation barrier, the ferrite must nucleate with a good match with at least one of the austenite grains with which it is in contact (Aaronson and Russel, 1981). Nucleation would therefore demand that all allotriomorphs should exhibit orientations within the Bain region. However, the original orientation distribution will be changed if the allotriomorphs grow into regions far from their original nucleation sites. This can happen if growth occurs at a higher rate along those austenite grains boundaries with which the ferrite has high energy (*i.e.*, high mobility) interfaces. Purdy (1978), using hot-stage transmission electron microscopy, has directly demonstrated the higher mobility of interfaces between ferrite and austenite which are randomly orientated. The smaller extent of ferrite penetration into the Bain region related austenite (Fig. 7.4), compared with growth into the other randomly orientated austenite grain is consistent with Purdy's work.

The orientation data (Tables 7.3 & 7.4) are consistent with the earlier studies of Ryder and Pitsch (1966) and King and Bell (1975). Although the present work reveals a rather smaller fraction of allotriomorphs with an orientation within the Bain region, any quantitative comparisons are doubtful since the crystallographic textures of the materials used are unlikely to be identical. The texture must influence the relative orientations of the austenite grains and hence the crystallography of the ferrite that forms subsequently. This may also explain why King and Bell found a larger fraction of allotriomorphs with a good match with both the adjacent austenite grains.

7.4.2 Ferrite Orientation with Respect to Both Adjacent Austenite Grains

It is only by coincidence that a ferrite grain nucleates with a reproducible orientation relationship with both of the austenite grains with which it is in contact. In general, it is only expected to have an orientation relationship with one of the parent austenite grains. It nevertheless seems reasonable that the ferrite should attempt to choose a variant of this orientation relation which allows the highest degree of matching with the other austenite grain, even though its orientation with the second grain may not be ideal.

The seven cases for which the ferrite was found to have an orientation within the Bain region (Tables 7.3 & 7.4) were analysed further to study whether the ferrite makes any attempt during nucleation to optimise lattice matching with both the austenite grains. For the other data, the crystallography suggests that the allotriomorphs have grown away from their original

Table 7.3. Summary of $\alpha - \gamma$ orientation relationship in alloy A1.

Number	θ	ϕ	Approx. Orientation
1a	4.04	3.2	KS/NW
1b	27.6	22.0	-
2a	0.0	5.0	NW
2b	18.1	32.1	-
3a	15.1	4.9	-
3b	13.7	13.6	-
4a	0.0	5.3	NW
4b	19.9	15.8	-
4c	35.3	33.5	-
5a	2.0	5.5	KS/NW
5b	20.5	16.4	-
6a	15.0	16.8	-
6b	18.9	22.5	-
7a	8.7	10.7	-
7b	24.5	10.1	-
8a	5.7	23.5	-
8b	28.9	28.5	-
9a	0.0	19.8	-
9b	24.3	10.6	-
10a	18.7	11.3	-
10b	26.4	26.4	-
11a	14.4	17.0	-
11b	25.5	23.8	-
12a	28.5	21.4	-
12b	21.4	30.8	-
13a	30.3	24.4	-
13b	24.4	26.8	-
14a	0.0	8.9	-
14b	2.7	28.7	-
15a	3.0	5.8	KS/NW
15b	6.9	5.3	$\simeq$ KS/NW

Table 7.4 Summary of $\alpha - \gamma$ orientation relationships for alloy A2.

Number	θ	ϕ	Approx. Orientation
1a	0.9	21.0	
1b	20.1	20.1	
2a	14.2	13.0	
2b	25.7	17.0	
3a	3.9	6.2	KS/NW
3b	27.3	26.2	
4a	3.8	5.6	KS/NW
4b	23.6	31.5	

sites, the observed orientations no longer being representative of the nucleation stage.

The degree of α/γ_2 fit was assessed by calculating the determinant of the matrix T, which represents the ratio of the volume of the unit cell of the Bollmann's O-lattice to that of volume of the unit cell of the reference crystal. The O-lattice is a set of points of perfect fit between the two crystal lattices which are allowed notionally to interpenetrate and fill all space. Hence, the smaller the value of the determinant, the better is the fit between the two crystals. The matrix T can be deduced from a knowledge of the deformation S which converts the lattice of one of the crystals into that of the other (the *reference* lattice). The deformation S can be deduced from a knowledge of the coordinate transformation matrix J (representing the orientation relationship) and an assumed correspondence matrix C. J is of course, measured experimentally whereas C is taken to be the Bain correspondence; the magnitude of the deformation S depends on the specific variant of the Bain correspondence, which in each case is chosen to be that which leads to the smallest determinant of T. Details of these methods can be found in reference (Christian, 1975).

Considering a $\gamma_1/\alpha/\gamma_2$ tricrystal, in which the γ_1/α orientation is within the Bain region, the symmetry of cubic crystals suggests that there are in general, twenty four variants of $(\alpha\ J\ \gamma_1)$.† Of these twenty four possibilities, one corresponds to the experimentally measured orientation, and the task here is to discover whether this particular variant of the orientation relationship also gives the best match with the crystal γ_2, *i.e.*, the one which gives the smallest value of the determinant of $(\gamma_2\ T\ \gamma_2)$, where

† The notation used here is due to Bowles and Mackenzie (1954), and suggests that J is a 3×3 coordinate transformation matrix describing the orientation relationship between α and γ_1. Each column of J represents the components of a basis vector of γ_1 in the basis α.

$$(\gamma_2\ T\ \gamma_2) = I - (\gamma_2\ C\ \alpha)(\alpha\ J\ \gamma_2). \tag{7.1}$$

In none of the seven cases examined did the allotriomorph seem to attempt to lattice match with both of the adjacent austenite grains. Thus, the experimental variant of the $(\alpha\ J\ \gamma_1)$ orientation did not correspond to the smallest possible value of the determinant of $(\gamma_2\ T\ \gamma_2)$, as illustrated in Fig. 7.7. The ratio of calculated minimum determinant value for $(\gamma_2\ T\ \gamma_2)$ for a given variant and the actual determinant value observed for $(\gamma_2\ T\ \gamma_2)$ is presented in Fig. 7.8, which summarises the variant analysis. The result is difficult to explain, but could indicate that the orientation of the austenite grain boundary plane might have an effect on the choice of the orientation variant (Aaronson and Russel, 1981).

7.4.3 Bainite/Austenite Grain Boundary Crystallography

The opportunity was taken during the allotriomorphic ferrite experiments, to measure also the orientations of grain boundary nucleated bainite and the adjacent austenite grains (Table 7.5). Similar to the results obtained for allotriomorphic ferrite, the bainite did not seem to choose an orientation variant with its parent austenite which gave the optimum matching with the other austenite grain.

Table 7.5: Alloy A1. Summary of bainite orientation relationship with the austenite grain in which it is growing (a), and with the grain on the other side of the boundary (b).

Number	θ	ϕ	Approx. Orientation
1a	0.0	5.3	NW
1b	10.5	10.3	-
2a	0.0	0.5	KS
2b	11.4	0.0	-
3a	0.7	0.0	KS
3b	3.3	0.0	KS/NW
4a	4.3	6.4	KS/NW
4b	0.7	5.3	NW
5a	0.06	0.0	KS
5b	14.9	0.0	-
6a	0.0	0.06	KS
6b	15.0	0.0	-

7.4.4 Detailed Examination of a Particular Allotriomorph

One of the experiments (Case 1, Table 7.3) revealed an exceptionally good example of an allotriomorph which exhibited microstructural features consistent with its α/γ_1 orientation being well within the Bain region, and a random α/γ_2 orientation (Fig. 7.4). With the γ_1 grain, the ferrite exhibited a very pronounced tendency to crystallographically facet, giving a clearly ledged transformation interface. Whether these ledges are growth ledges, or simply facetting which results from tendency of the particle to minimise interfacial energy, can only be decided by observing the growth. Their non-uniform height and spacing (Fig. 7.9) is consistent with theory for ledged growth (Atkinson, 1982), but such variations can also be expected from facetting. The important point is that the facets represent planes of low interfacial energy around the particle.

The crystallographic indices of the facet planes were measured using a method of trace analysis which avoids ambiguity. Because the interface planes were inclined to the foil surface, their projected widths within the foil and contrast conditions can be used to measure their inclinations, which can in turn be used to fix the interface plane uniquely; the fringe contrast also helps to fix the sense of inclination of the interface plane. The results are plotted on Fig. 7.10, which also illustrates the interfacial energy minima calculated by Ecob and Ralph (1981). It is evident from Fig. 7.10, that within the limits of experimental error, the present data are approximately consistent with those calculations.

A further interesting feature is that the α/γ_1 side of the boundary has been able to nucleate a plate of bainite (Fig. 7.4 & 7.11) during the second stage of the heat-treatment (below the bainite-start temperature). This is consistent with the discussion earlier that only allotriomorphs whose orientation lies within the Bain region can be active in nucleating the products of displacive transformation (*e.g.* bainite, Widmanstätten ferrite). By contrast, a transformation-free region is observed on the other side (α/γ_2) where the allotriomorph is randomly orientated. It is also interesting to note that the trace of the bainite habit plane for the plate nucleated from the allotriomorph does not coincide with the facet planes on the allotriomorph (Fig. 7.11). The bainite habit plane should be determined by the minimisation of strain energy due to the shape change accompanying transformation, rather than interfacial energy minimisation.

7.4.5 Chemical Composition of Allotriomorphic Ferrite

It is of interest to examine the chemical composition of the allotriomorphic ferrite formed in the two alloys because the alloys A1 and A2 had respectively been heat-treated at temperatures above and below the paraequilibrium Ae3' curve of the phase diagram (Fig. 7.12). Paraequilibrium is a condition of constrained equilibrium in which the iron to substitutional solute atom ratio is constant everywhere during transformation, but subject to that constraint,

the carbon attains the same chemical potential in all phases. Thus, the Ae3' curve defines the composition of the austenite which is in paraequilibrium with ferrite. The curves presented in Fig. 7.12, and the thermodynamic calculations presented in Table 7.2, were calculated as in references (MTDATA, 1989 and Bhadeshia and Edmonds, 1980). The experimental data presented in Table 7.2 represent the bulk chemical compositions of the ferrite allotriomorphs, and conclusively demonstrate that both the manganese and silicon partition during the growth of ferrite in both the alloys, for the transformation conditions described earlier. Furthermore, although partitioning is found, its extent is less than that expected from equilibrium considerations (Table 7.2) and the growth process is best described as *nonequilibrium.*

For the transformation conditions used, it is thermodynamically impossible for the ferrite in alloy A1 to grow by a paraequilibrium mechanism, so that the partitioning of manganese and silicon is necessary during transformation. Since alloy A2 was transformed below the Ae3' phase boundary (Fig. 7.12), it is *thermodynamically* possible for the ferrite to form with paraequilibrium; this does not however, rule out growth with local equilibrium at the interface, or indeed with any of an infinite set of conditions between equilibrium and paraequilibrium. The exact mode of transformation must be decided by kinetic considerations. A method for estimating the transition from equilibrium to paraequilibrium involves the calculation of the extent z of the diffusion field of the solute element (Coates, 1973a):

$$z \simeq 2D/v \tag{7.2}$$

where D is the diffusivity of the solute concerned in the parent phase, and v is the interfacial velocity, which for the present circumstances is time dependent ($v = \alpha_1 t^{-0.5}$, where α_1 is the one–dimensional parabolic thickening rate constant and t is the growth time). Coates suggested that if z is found to be less than about 1 nm, then growth could be assumed to occur by a paraequilibrium mode, since the diffusion distance is then negligible.

The velocity was estimated by measuring the mean allotriomorph half–thickness (q) and dividing by the isothermal transformation time. This might lead to an underestimation of v since an incubation period may be necessary before the nucleation of ferrite, an approximation which would lead to an overestimation of z. The values of z were found to be $z_{Mn} \simeq 18\,\text{nm}$ and $z_{Si} \simeq 4\,\text{nm}$ for alloy A1 in which the transformation was carried out at the higher temperature (above Ae3'). For alloy A2, on the other hand, both of the calculated diffusion distances were found to be incredibly small at $z_{Mn} \simeq 8 \times 10^{-2}\,\text{nm}$ and $z_{Si} \simeq 0.14\,\text{nm}$. In contradiction to the experimental evidence for alloy A2, this suggests that allotriomorphic ferrite growth should occur by a paraequilibrium mechanism.

As first pointed out by Coates, the diffusion distance criterion for assessing the onset of

paraequilibrium growth is unlikely to be correct, since conventional diffusion theory breaks down as the concentration gradients become large. Hillert (1981) has also pointed out that the criterion fails to predict the experimental observations on pearlite and massive ferrite.

Aziz (1982) has developed a model for solute trapping during rapid solidification, which is likely to be a better representation of nonequilibrium growth (Olson *et al.*, 1990). If the actual ratio (partition coefficient) of the solute concentration in the product to that in the parent phase at the interface is written k_p, and the equilibrium ratio k_e, he finds that

$$k_p = (1 + \beta k_e)/(1 + \beta) \tag{7.3}$$

where $\beta = D/(v\lambda)$, λ being the intersite diffusion distance assumed to be 0.25 nm. As k_p tends towards unity, growth tends towards paraequilibrium. For the present experiments, assuming that the measured ferrite concentration can be used to estimate k_p,† the theory is found to predict correctly that substitutional solute partitioning should occur during the growth of ferrite in alloy A2. The partition coefficients were calculated to be $k_p^{Mn} \simeq 0.7$ and $k_p^{Si} \simeq 1.7$.

7.5 Summary & Conclusions

By using a steel containing a large silicon concentration, and a two–stage heat treatment procedure, it has been possible to produce a microstructure consisting of allotriomorphic ferrite, bainitic ferrite and retained austenite. This permitted a direct examination of the crystallography of grain boundary allotriomorphs of ferrite. It is found that the fraction of allotriomorphs which have an orientation (with the parent austenite) which is in the Bain region is rather small. This has implications on the theory for the prediction of microstructure in steel welds, where a thin layer of allotriomorphic ferrite is required to promote the intragranular formation of acicular ferrite, as long as it can be prevented from nucleating Widmanstätten ferrite at the same time. This qualitative conclusion has to be backed by further research before the fraction of active allotriomorphs can be predicted. Such work must consider the role of crystallographic texture in the parent austenite, and of its subsequent rate of transformation to allotriomorphic ferrite.

Most of the allotriomorphs do not seem to attempt to maximise lattice matching with both of the grains with which they are in contact, and it is speculated that this might be due to an influence of austenite grain boundary orientation in determining variant selection.

It has been shown that the transition to paraequlibrium growth as the transformation temperature is reduced, cannot be predicted by estimating the extent of the solute diffusion

† It is really the concentrations at the transformation interface which are of relevance, so that the calculated values of k_p cannot be compared directly with our experimental data, although they can certainly be used to indicate whether growth should involve a substantial degree of partitioning.

field in the austenite during allotriomorphic ferrite growth. A possible way forward would be to utilise solute trapping theory, in a manner applied already to coupled diffusional/displacive transformations (Olson *et al.*, 1990), to predict the partitioning coefficient as a function of undercooling below the equilibrium transformation temperature.

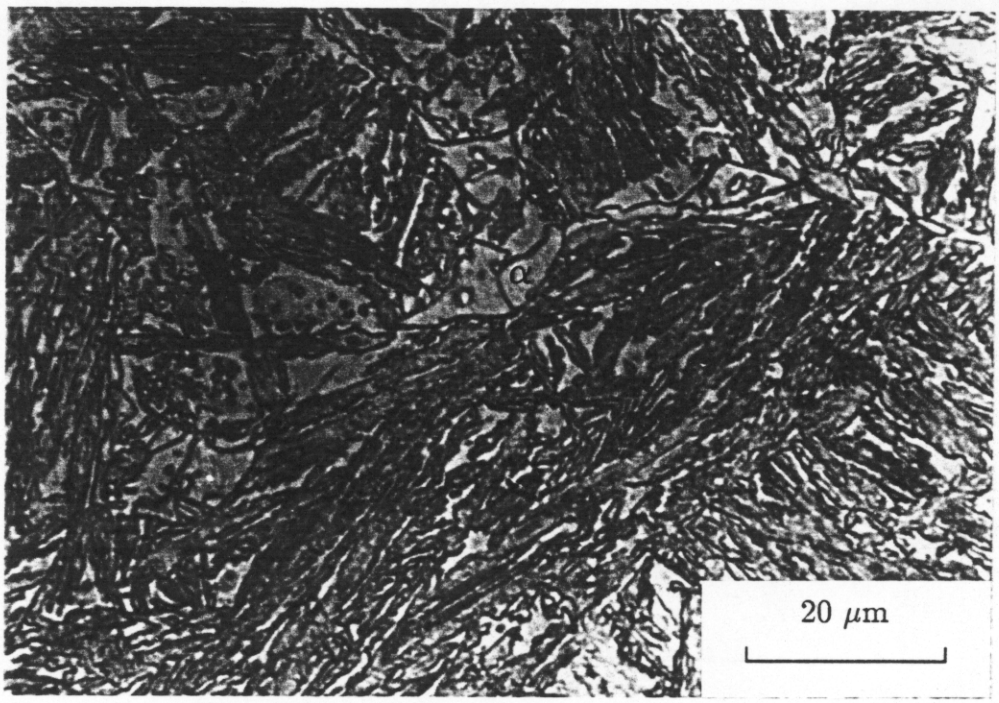

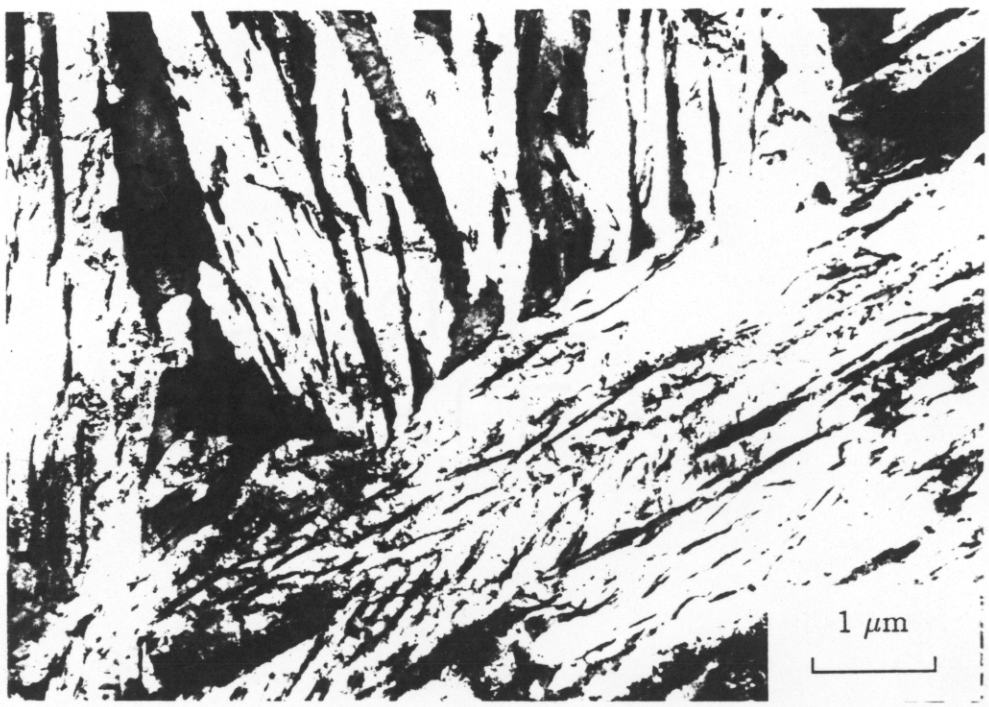

Fig. 7.1 Microstructure observed in alloy A1 after the step heat treatment as mentioned in Table 7.1

a. Optical micrograph of alloy A1, indicating the allotriomorphic ferrite all along the austenite grain boundaries.

b. Transmission electron micrograph of A1, illustrating the sheaf structure of bainite.

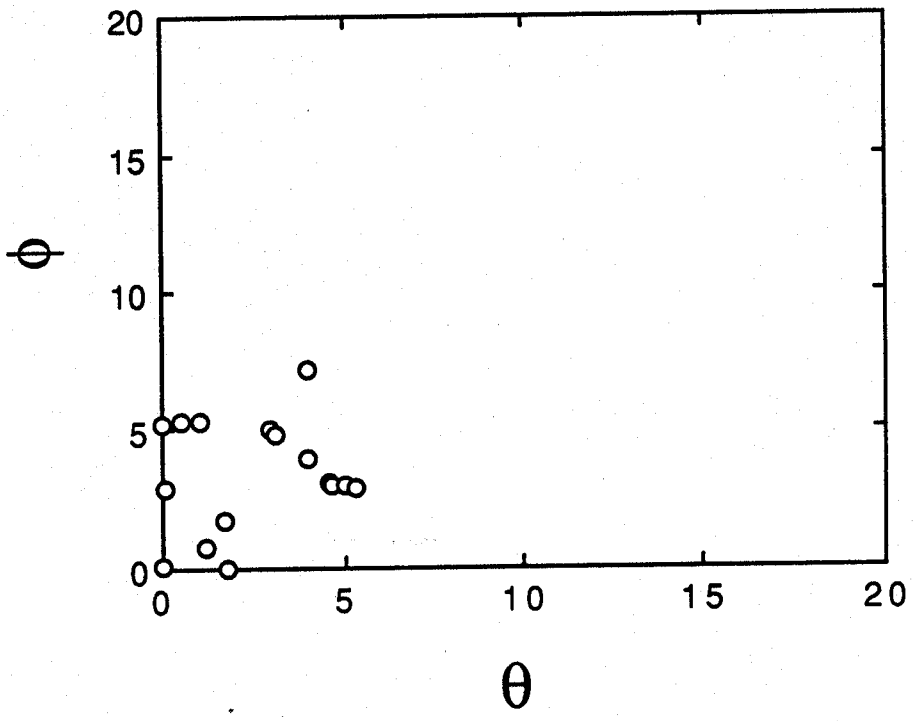

Fig. 7.2 Graphical presentation of summary of $\alpha - \gamma$ orientation relationship for 16 cases of bainite, where θ is the angle between $\{ 1\,1\,1 \}_\gamma - \{ 0\,1\,1 \}_\alpha$ and ϕ is the angle between $< 1\,0\,\bar{1} >_\gamma - < 1\,1\,\bar{1} >_\alpha$.

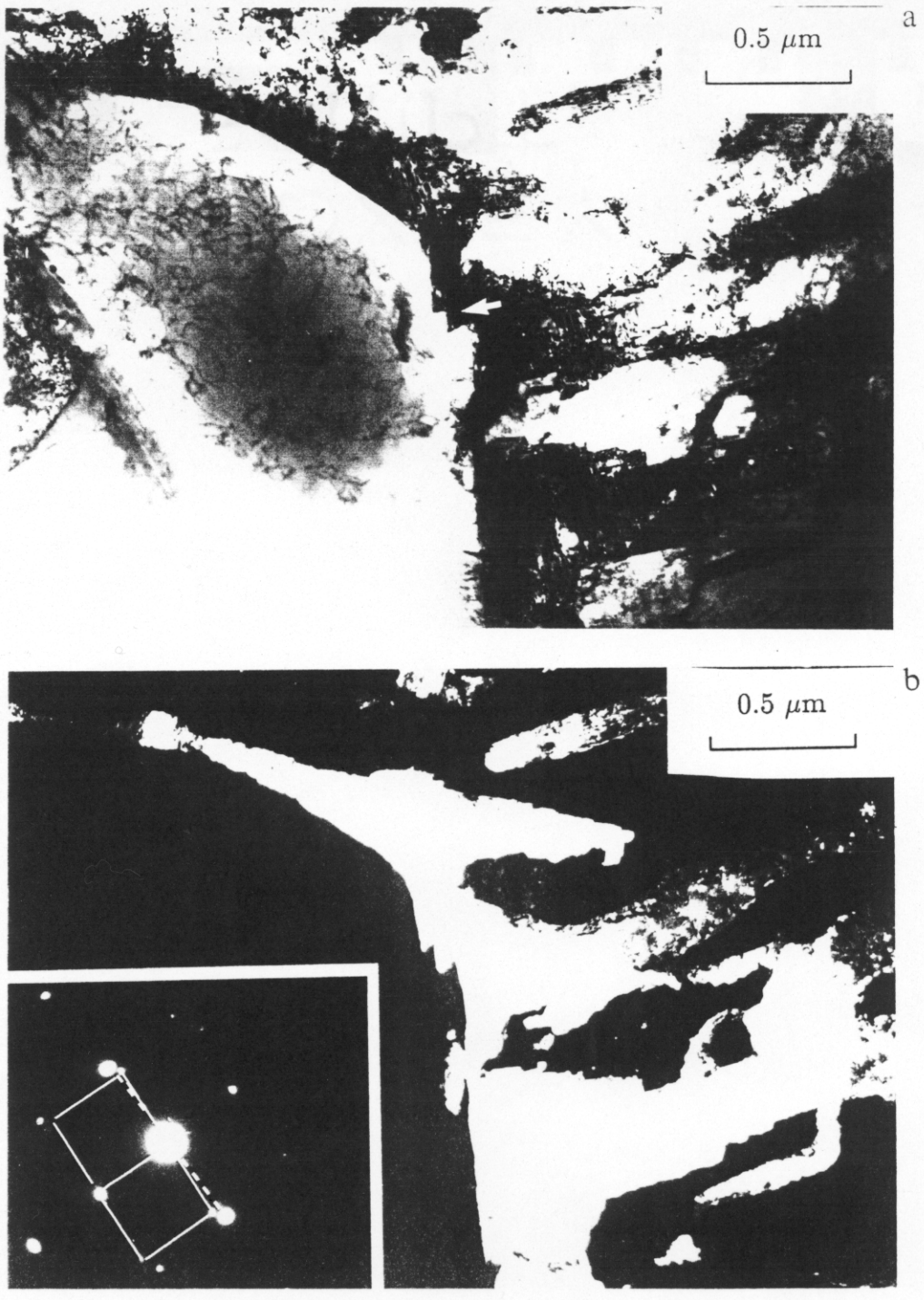

Fig. 7.3 Microstructure obtained in alloy A1 after the step heat treatment. (a) Bright field micrograph illustrating allotriomorphic ferrite, bainite and retained austenite, (b) corresponding dark field micrograph for the residual austenite. The inset is the diffraction pattern from the allotriomorphic ferrite and austenite (solid line is ferrite < 001 > zone axis and dotted line is austenite).

Fig. 7.4 (a) Bright field electron micrograph exhibiting an allotriomorphic ferrite nucleated from austenite grain boundary (marked as B), and bainitic sheaves growing from austenite grain boundary and also within the grain. (b) Diffraction pattern from the allotriomorphic ferrite and γ_1 a near KS/NW orientation relation, (c) the diffraction pattern of austenite γ_2 from the random orientation side of allotriomorphic ferrite, consisting of other reflections due to bainitic ferrite also. The γ_2 reflections are used for finding orientation relation ($\alpha J \gamma_2$), by overlapping the two diffraction patterns appropriately (see overleaf).


B
1 μm
(a)

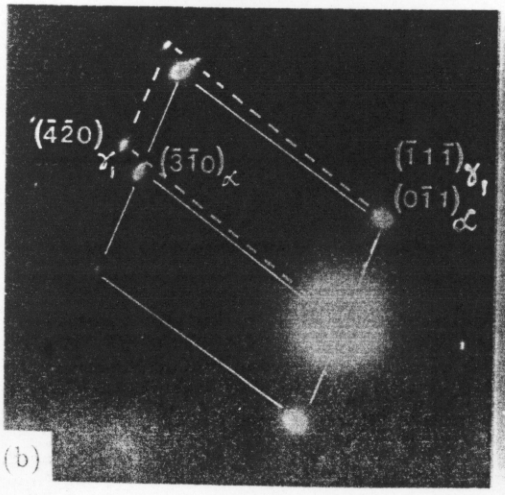
(4̄2̄0)γ
(3̄1̄0)α
(1̄1 1̄)γ
(0 1̄ 1)α
(b)

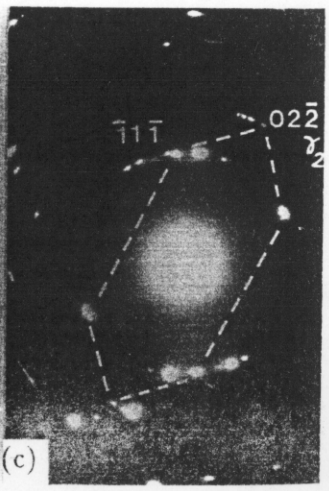
1̄1 1̄
02 2̄
γ
(c)

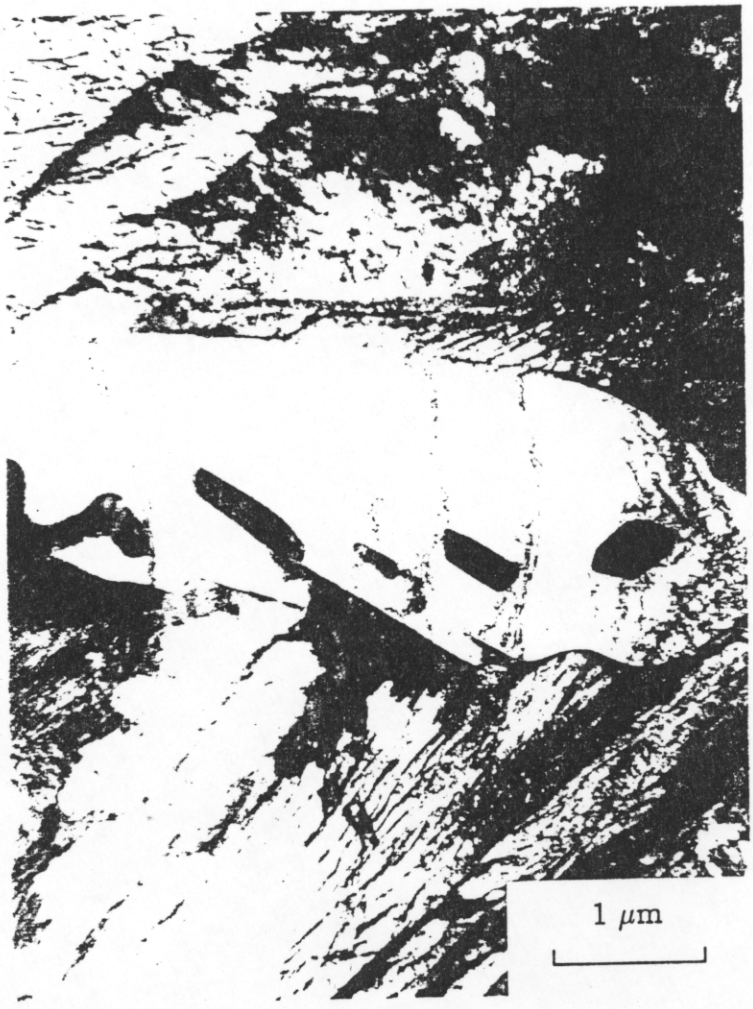

Fig. 7.5 An allotriomorphic ferrite in alloy A1 with carbides. The morphology suggest that the precipitation might have occurred during transformation to ferrite, explaining the apparent coverage by single allotriomorphic grain.

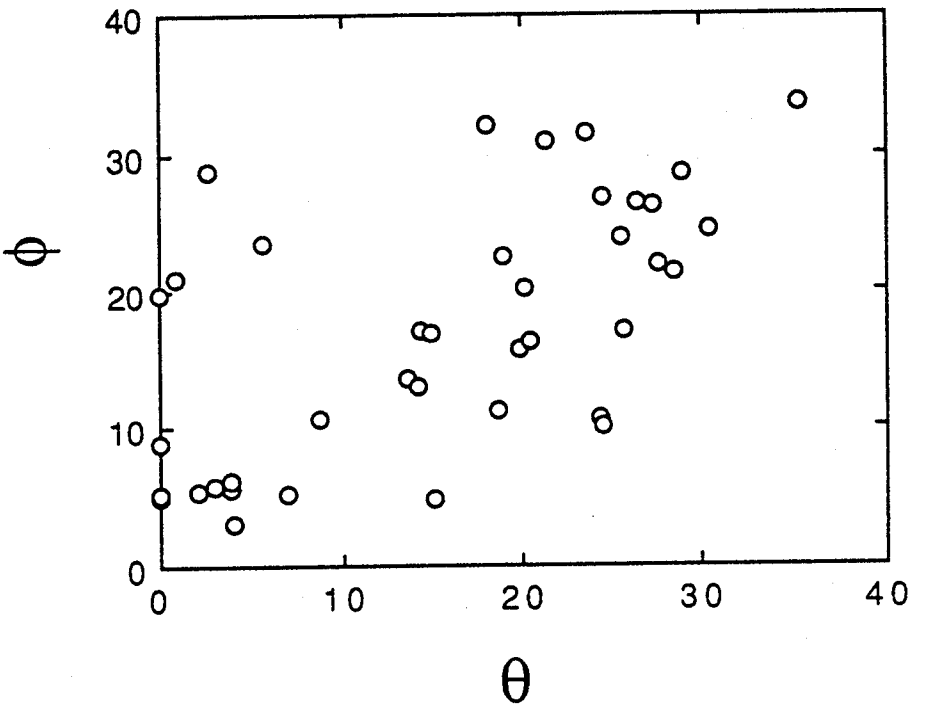

Fig. 7.6 Graphical presentation of summary of $\alpha - \gamma$ orientation relationship, data from Table 7.3 & 7.4, where θ is the angle between $\{ 1\ 1\ 1 \}_\gamma - \{ 0\ 1\ 1 \}_\alpha$ and ϕ is the angle between $< 1\ 0\ \bar{1} >_\gamma - < 1\ 1\ \bar{1} >_\alpha$.

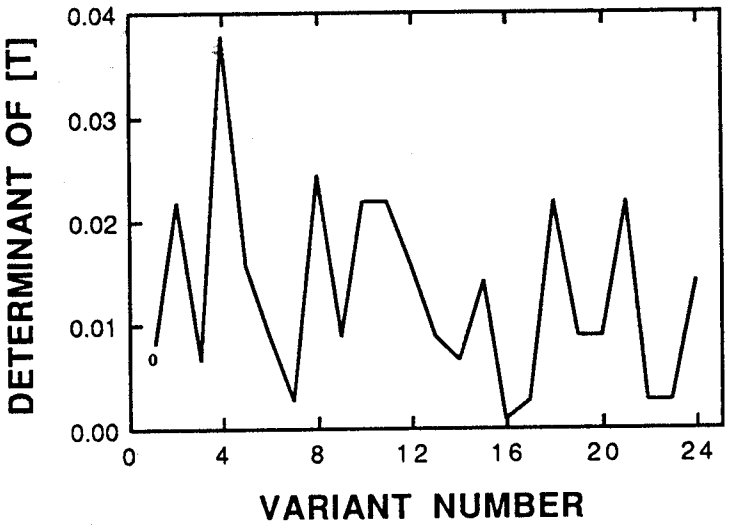

Fig. 7.7 Plot of variation of determinant value of T matrix, as discussed in the text. The point (for variant 1) indicates the determinant of T matrix obtained using the experimentally observed orientation relationship, $(\alpha J \gamma_2)$.

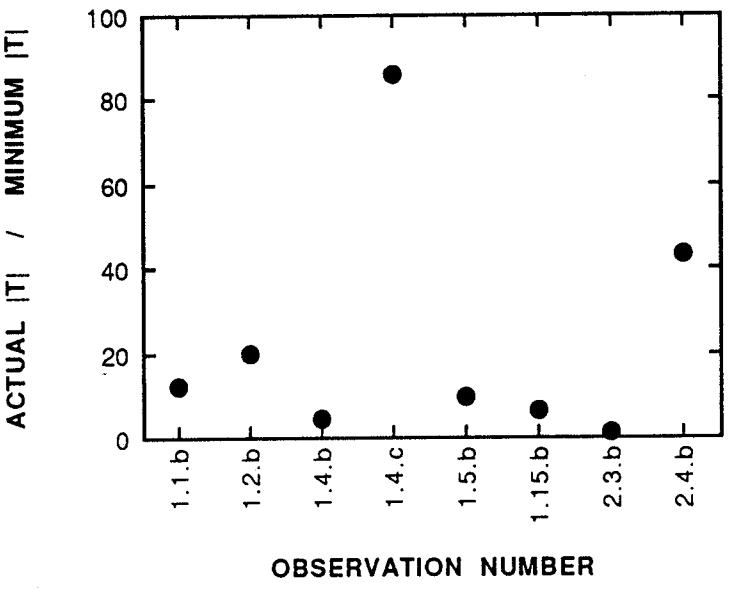

Fig. 7.8 Summary of variant analysis on allotriomorphic ferrites which exhibited near KS/NW with one of the austenite grain. The ratio of determinant value of observed $(\gamma_2 T \gamma_2)$ to that of calculated minimum determinant value is plotted for all the cases. Prefix 1 & 2 correspond to the data from alloy A1 and A2, respectively (Tables 7.3 & 7.4); ideally a value of 1 is expected to indicate a good fitting with γ_2 for a given $(\alpha J \gamma_1)$ variant.

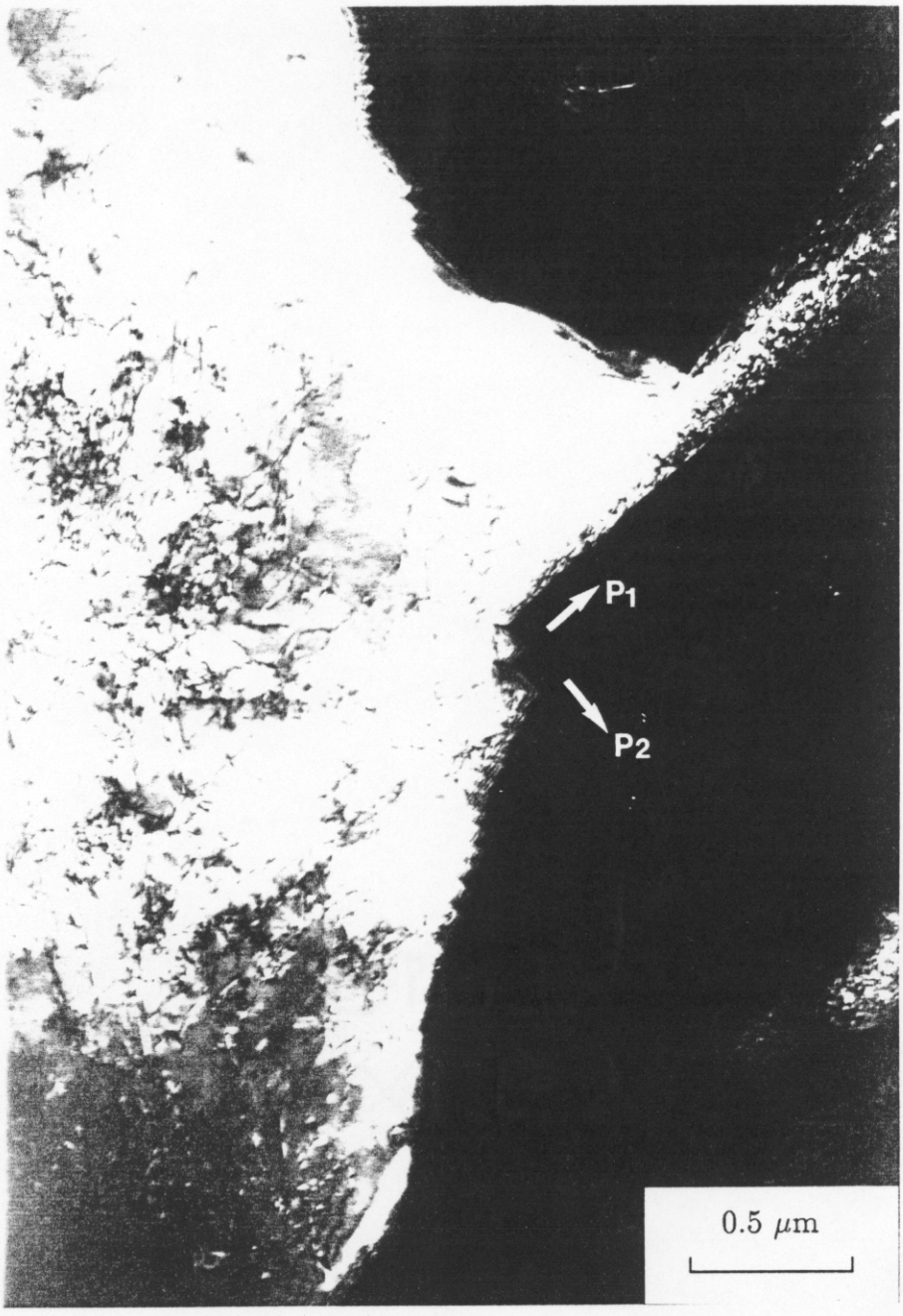

Fig. 7.9 The micrograph of the interface which showed KS/NW relation with the austenite, exhibiting ledge type faceted interface. The ledge height can be seen to vary over the width of the ferrite, apparently increasing towards the nucleation site of bainite.

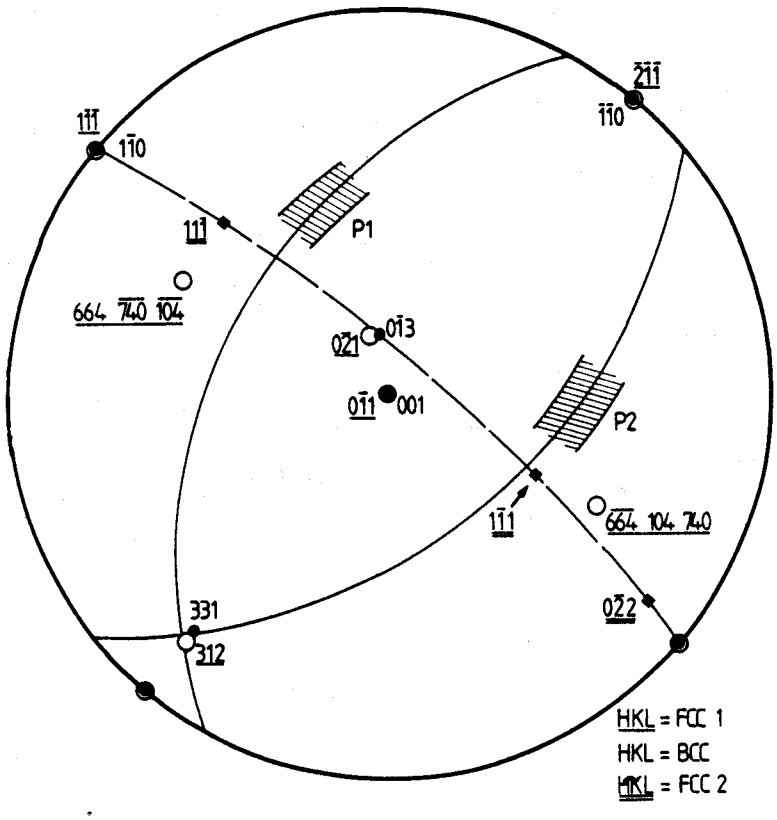

Fig. 7.10 Stereogram plot of interface plane calculations for the allotriomorphic ferrite interface which exhibited KS/NW (case 1 of Table 7.3), and exhibited ledge type interface. The stereogram is overlap of $[\ 0\ 0\ 1\ ]_{\alpha}$ and $[\ 0\ \bar{1}\ 1\ ]_{\gamma}$ zone axes. The low energy equilibrium interface planes calculated by Ecob and Ralph (1981) are also plotted.